The University of Nottingham
UNITED KINGDOM • CHINA • MALAYSIA

School of Life Sciences

Axon diameter determines the mouse optic nerve compound action potential profile in response to varying stimulus frequency

Amy Jean Hopper

Submitted to the University of Nottingham for a Master of Research Degree in Neuroscience

Supervisors: Dr Angus Brown and Dr Rebecca Trueman

Abstract

The mouse optic nerve (MON) is a central white matter tract, whose axons range in diameter from 0.2 to 2.7 μm. In the adult animal all the axons are myelinated, conferring increased conduction velocity. Increased conduction velocity can also be achieved by increasing axon diameter. However, current thinking considers that although large axons conduct quickly, this is unlikely to be the primary function of large axons in the MON. The surface area to volume considerations, and the consistent mitochondrial density in the axoplasm, result in larger axons containing an increased number of mitochondria, capable of efficiently dealing with energy perturbations and maintaining ion equilibration.

The MON is an ideal model to investigate the effect of high frequency firing on the ability of axons to sustain firing. There is a clear differentiation between the three peaks of the compound action potential (CAP), which is predicted to relate to large, intermediate, and small axon, based on the premise that axon diameter dictates conduction velocity. The basal firing rate of the MON is 5 Hz. Larger axons can propagate action potentials at much higher frequencies with no loss of fidelity, whereas smaller axons cannot. This distinction between axons in the same tract is an intriguing observation worthy of investigation. The separation of the CAP profile into distinct peaks allows us to measure how the peaks respond to the same stimulus. Indeed, under metabolic challenge achieved via high frequency firing, we measured a differential fall in the third peak (small axons), compared to the second (intermediate), and then the first (large). Following 5 minutes of 100 Hz stimulus, peak 1 fell to 70%, peak 2 to 40%, and peak 3 to 15%, of the baseline peak amplitude.

Based on the classic electrophysiology experiments which modelled the depolarising effects of elevated potassium on membrane potential, it is reasonable to assume K^+ efflux from the axons underlies the fall in the CAP. To investigate this, we used a two-pronged approach. First, we used a direct method to measure the extracellular potassium ($[K^+]_o$) with ion sensitive microelectrodes, supporting previous data showing that $[K^+]_o$ does not significantly increase in response to high frequency firing. Second, we used an indirect method, increasing the artificial cerebrospinal fluid $[K^+]$ to determine the concentration at which the CAP peak amplitude started to reduce. We show that the CAP peaks fell at $[K^+]$ higher than those achieved in response to 5 minutes stimulus of 100 Hz stimulus: 4.5 mM. This suggests an alternate cause of CAP failure.

High intracellular sodium ($[Na^+]_i$) is a likely candidate, however technical considerations limit the ability to measure this directly in individual axons. Therefore, we used an indirect method by decreasing the extracellular $[Na^+]$, which caused the CAP to fall in amplitude. We quantified this failure using the Nernst equation, which subsequently allowed us to estimate the elevations in $[Na^+]_i$ that would occur as a result of high frequency firing, when extracellular $[Na^+]$ remains constant. Following 5 minutes of 100 Hz, we predicted that $[Na^+]_i$ rises to 23 mM for peak 1, 42 mM for peak 2, and 64 mM for peak 3.

We propose that the differential effect of frequency firing on large axons (compared to small axons) is due to the surface area to volume ratio providing an increased mitochondrial count, conferring an increased capacity to support firing under a metabolic challenge.

Acknowledgements

I would like to thank my primary supervisor, Dr Angus Brown, for his time and dedication spent training me this year, from teaching me how to re-build an electrophysiology lab, to publish papers. I am grateful, also, to my lab-partner Hana Beswick-Jones, without whom this year wouldn't have been half as enjoyable.

Table of Contents

1 Introduction

1.1 The golden era of electrophysiology

Action potentials are intrinsic to excitable cells in most multicellular eukaryotic organisms from vertebrates to plants, facilitating communication between cells, tissues, and organs. Physiology aims to explore and understand how these mechanisms fundamentally work, to help uncover how systems respond and adapt to changes in the environment. The 'golden era' for neuro-electrophysiology lasted four decades, starting in the 1930s with the first intracellular recording of the action potential conducted by two prominent British pioneers of physiology; Alan Hodgkin and Andrew Huxley. This dynamic duo used ingenious methodologies, combining both pre-existing and novel experimental and mathematical techniques, to explore the underlying mechanism of the action potential. The action potential results from current movement carried by ions; the flow of current across the membrane results in changes to the membrane potential (Hodgkin and Huxley, 1952). Hodgkin and Huxley used voltage recordings to delineate the currents contributing to the action potential and determined that it is driven by an influx of sodium ions and an efflux of potassium ions. The application of the voltage clamp and double-pulse protocols was widely copied leading to a 'boom' in electrophysiology, with labs across the globe dedicating time into exploring electrical activity. Multicellular organisms require action potentials as a fundamental internal signalling system, therefore understanding the mechanistic effects that occur under normal physiological states could elucidate the ways in which nerve conduction is affected in diseases such as multiple sclerosis and neuritis. This form of research explores the influence of metabolic stress on axons, from metabolic insults that strongly affect the function of nerves like hypoglycaemia (Brown *et al.*, 2003), to high frequency firing which confers a metabolic challenge on axons (used in this thesis). Many important questions remain unresolved, and *ex vivo* rodent nerve preparations such as the mouse optic nerve (MON) could be a key model to provide answers. It appears pertinent to consider changes to axonal firing ability, particularly in mammalian nerves, due to the differences in the physiological model organism used in early action potential research: the squid, Loliginidae (Hodgkin and Katz, 1949). Despite advances in technology and optimisation of experimental equipment from the 1950s, it remains technically difficult, if not impossible, to conduct intracellular recordings from the vertebrate axons due to their small size. Therefore, explorations of mammalian nerve firing often utilise indirect methods proposed and adapted by Hodgkin and Huxley, alongside various electrode techniques, to explore the effect of changes to physiological conditions on action potential propagation.

Here the chronological journey through time is described as follows (Figure 1), a) the initial development of ionic gradients in the first cells and membrane proteins required to maintain such differences, b) the exploitation of voltage gradients for the action potential in excitable cells explained through the Nernst equation, c) the evolution of myelin to reduce the metabolic demand on neurons, d) the role-switch of myelin to increase conduction velocity, e) how large axons similarly evolved to increase conduction velocity, f) exploring the need for large axons in mammalian nerves such as the MON, g) to how electrophysiology can be used to explore the metabolic reason for different diameters (this study).

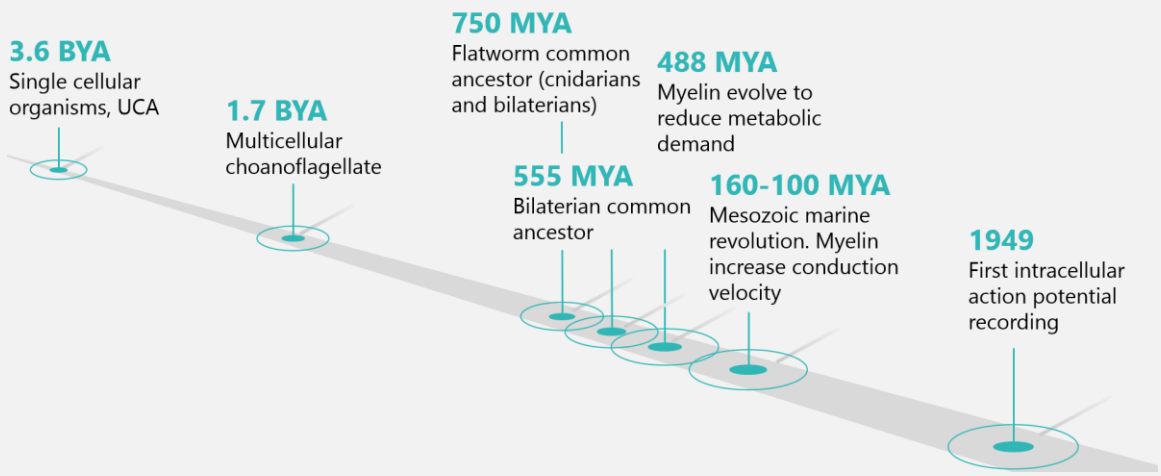

Figure 1. Timeline depicting key events in the evolution of nervous tissue. The time-span of purely single celled organisms including the universal common ancestor (UCA) is the same as the time-span between the first multi-cellular organism and present life on earth.

1.2 Evolutionary conservation of ionic concentrations and underlying mechanisms of the action potential

Although obsolete nowadays, research using the squid giant axon expedited understanding of the action potential and key processes that occur universally in axons. The ionic gradients formed across excitable cell membranes in both squid and mammals have been evolutionarily conserved from the first cells on earth. The universal common ancestor (UCA) theory proposes that all life originated from a single cell ~3.6 billion years ago (BYA), and following the chemistry conservation principle this prokaryotic cell likely existed in the oceans. It is widely accepted that the oceans formed from atmospheric cooling facilitating water vapour condensation (Pinti, 2005). The salinity content of the oceans during the Proterozoic era (2.5 BYA to 538.8 million years ago (MYA)) has been estimated to have retained a sodium and chloride ratio similar to today's oceans, based on samples taken from ancient rock formations (de Ronde *et al.*, 1997; Martin *et al.*, 2006). These samples also retain a low potassium and magnesium content. The ion concentrations present in the cytosol of most cellular life is contrary to these relative ratios, see Figure 2 for the relative concentrations. Note how, despite the difference in absolute values, the ratios of ions in squid and mammalian axons have remained consistent over 750 MYA from their common ancestor. Macallum's investigations into cellular ion content lead to the theory that cells evolved in high potassium habitats, especially since all modern eukaryotic cells, bacteria and archaea have a higher potassium prevalence than sodium (Macallum, 1926; Mulkidjanian *et al.*, 2012). Since the ocean has high sodium, and low fundamental magnesium, phosphate, and silica, the two more likely locations for the evolution of a UCA are deep geothermal vents or rock pools (Mulkidjanian *et al.*, 2012).

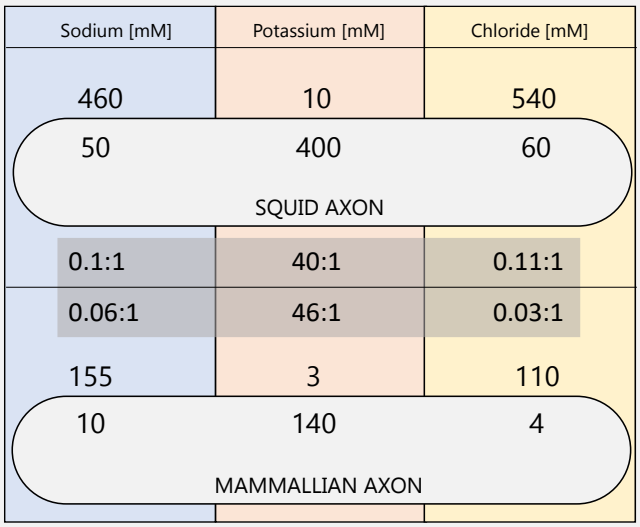

Figure 2. Conservation of relative ionic gradients from squid to mammalian axons. Comparison of absolute concentrations, yet the ratios between the intracellular and extracellular ion concentrations of sodium (blue), potassium (orange), and chloride (yellow), in mM, have been conserved (ratios in grey box).

Evolutionarily ancient cells require a compartmentalised internal environment to support normal cell homeostasis, which coincidentally produces ionic and voltage gradients, a property exploited by excitable cells. Selection for the formation of tight biological membranes prevents passive sodium influx that would occur given the high salinity content of the extracellular environment (Skulachev, 1988). Modern cell membranes are proton-tight yet the underlying increased complexity in structure likely evolved from changes to early sodium tight membranes (Skulachev, 1988). Nucleotides and genetic replication is inhibited by high sodium concentrations, providing an evolutionary pressure for low internal sodium content in order for cell division to occur. This supports the theory describing life originating in rock pools with high potassium content which supports genomic stability and the formation of fatty-acid membranes. Permeability pathways for specific ions evolved in the form of ionic pores, channels, and pumps, to maintain the ionic concentration gradients and osmolarity. The high intracellular ion content promotes the passive efflux of potassium through 'leak' channels in the membrane, which exist across species originating from metazoan cells (Jegla *et al.*, 1995). Potassium and calcium channels evolved first, with sodium channel structure indicating it evolved from these primitive membrane channel proteins (Hille, 1989; Liebeskind *et al.*, 2011). These voltage gated channels convey sodium influx and potassium efflux, down the ions' respective electrochemical gradients. Following early cells moving into the oceans, the increasing salinity in the external environment could have added to the pressure for cells to pump these ions in the opposite direction, including pumping excess sodium out of the cell. Ancestral ATPases such as the Vacuolar-type ATPases that transport sodium bidirectionally could have evolved to facilitate energy production via ATP synthesis alongside sodium influx, and gradually favoured the active movement of sodium out (Mulkidjanian *et al.*, 2007). V- or F- type ATPases (Na/K pump) are ubiquitous to life and would likely be present in the UCA (Mulkidjanian *et al.*, 2008). The co-evolution of ATP-dependent pumps, alongside the ion-

selective channels, forms and maintains the resting membrane potential, at the expense of being an energetically costly process. Cell membranes have to support the volume and composition of the cytosol contained within, a problem that is exacerbated by weak and fragile membranes (Armstrong, 2003). As mentioned and depicted in Figure 2 the extracellular environment contains a high concentration of chloride ions (Cl^-) and control over the intracellular content is vital for osmotic stabilisation. The osmotic capacity of cells is controlled by alterations in the osmotic differences across the membrane, by reducing the internal ion content through the active Na/K pump (Danowski, 1941), or through lowering intracellular chloride content (Armstrong, 2003).

Expanding on the UCA cell theory, Ernst Haeckel proposed this cell existed as a single ancestral choanoflagellate-like cell which formed colonies, from which individual cells differentiated to have specific functional roles for the organism (Haeckel, 1892). See Figure 1 to appreciate the time-span between single and multicellular organism evolution. Libeskind *et al.* (2011) determine that the presence of many ion channels involved in the action potential of excitable cells pre-date multicellular organisms such as this choanoflagellate ancestor which occurred around 1.7 billion years ago. Communication within multicellular organisms necessitates mechanisms like the action potential, utilising the potential of ion movement to drive signalling to distances further than diffusion alone could supply. The first nervous system evolved as a nerve net in Cnidaria, with genomic analysis showing how many similar voltage gated ion channels are present from this stage. Types and variations of nervous systems expanded from this template through the Cryogenium to Ediacaran periods, with the common bilaterian ancestor occurring around 555 million years ago, alongside cnidarians and ctenophores (Erwin & Davidson, 2002). Further genetic analysis shows a large degree of independent evolution in these genes encoding ion channels across early species, despite nervous systems showing no apparent phenotypic change. A key example representing the variety in underlying ionic processes that retain conserved action potential properties, comes from investigating the class Cephalopoda; the close relatives of squid, octopus (Octopoda) have calcium and potassium currents, as opposed to sodium and potassium (Rokni & Hochner, 2002; Hanke & Kelber, 2020). Future references to the action potential in this thesis assume sodium and potassium currents, found across most systems, but importantly squid and mammals. This highlights the fundamental importance of ion channels underpinning excitable cell action potential production and the evolutionary conservation of similar channels and mechanisms, enabling certain electrophysiological research using genera such as Loligo to remain applicable to mammalian systems at a rudimentary level.

1.3 Origin of the Nernst potential

Biological membranes compartmentalise the internal cellular environment and control a state of constant flux which maintains ionic potential gradients and the outward movement of signalling molecules and waste products. Equations have been explored to define the activity of these membranes, the most important of which being the application of the Nernst equation to the action potential (Eq. 1). The Nernst equation applies to individual ions and the reversal potential is where no net flux of an ion occurs. Astrocyte membranes are exclusively permeable to potassium, therefore changes to the potassium ion concentrations have a direct

effect on the membrane potential; this is a property pivotal to glial buffering of extracellular ions, explored in more detail in section 1.6. Mammalian axon membranes are permeable to several ions simultaneously, therefore the membrane potential is an aggregate of the contributions of these ions. The ion to which the membrane is most permeable primarily determines the membrane potential, which is potassium in mammalian and squid axons, so the resting membrane potential lies closer to the reversal potential for potassium (E_K) compared to other ions. The permeability of the membrane alters during the action potential, such that in depolarisation the membrane is more permeable to sodium ions (E_{Na}) so approaches +55 mV (Eq. 2), and in repolarisation the potassium permeability is highest so the potential approaches the E_K at -103. mV (Eq. 3).

$$E_x = \frac{RT}{zF} . log_{10}\left(\frac{[x]_o}{[x]_i}\right) \quad \text{Eq. 1}$$

$$E_{Na} = 61.5. log_{10}\left(\frac{155}{20}\right) = +55\, mV \quad \text{Eq. 2}$$

$$E_K = 61.5. log_{10}\left(\frac{3}{140}\right) = -103\, mV \quad \text{Eq. 3}$$

A comprehensive understanding of the Nernst equation is pivotal to understanding and analysing action potential recordings, as it underpins most electrophysiology research. Hodgkin and Huxley necessitated using complex mathematical knowledge to combat the difficulty of solving research problems 30 years prior to the technological advances that enable current experimental recordings. Nowadays, research utilises the background work explored by these physiologists alongside using electrodes to study the extracellular ionic concentration changes and the compound action potential (CAP). Hodgkin and Huxley unveiled the biphasic properties of the sodium currents, acknowledging sodium current inactivation, now known to be due to channel inactivation. This prevents continuous channel opening and excessive-influx of sodium, which allows ionic gradients to re-equilibrate and maintains the signal amplitude of future action potentials i.e. there is no degradation of the signal amplitude during trains of stimuli.

Maintenance of the ion gradients after activity in neurons is regulated by the Na/K pumps, simultaneously moving three sodium ions out and two potassium ions into the cell. The pump's activity changes depending upon the amount of ion movement required to restore the gradients. One ATP is required for the movement of those five ions. Considering the number of ions that move in one action potential, action potentials per axon, and neurons firing at once, the amount of energy required to reinstate the ionic gradients in a nerve tract increases greatly. Furthermore, the distribution, number, capacity, and rate of the Na/K pump affects the metabolic demand (the expression of the Na/K pump limits the ability for the axon to fire more). It has been estimated that although taking up just 2% of human body weight, the brain surmises 20% of the total human resting metabolic rate, with these pumps alone using 28% of the oxidative metabolic requirement of the body (Rolfe & Brown, 1997). This highlights the evolutionary value of membranes, channels, and pumps that facilitate maintenance of the ionic gradients, in resting and active states, to support the continued fidelity of action potentials.

One defining characteristic of the action potential is that propagation retains the initial amplitude, in an all-or-nothing response. Early experiments by Hodgkin, Huxley, and Frankenhaeuser showed that the action potential can decay over time if the ionic concentrations bathing the axon are changed (Frankenhaeuser & Hodgkin, 1956). Under normal physiological conditions, we assume that mammalian axons function the same and cope with action potential firing as this is an innate and important process. However, models and experiments using high frequency firing, and use of changes to the bathing artificial cerebrospinal (aCSF) can aid investigations into the processes that facilitate action potential propagation. More detail into these types of research is explored in later sections.

1.4 The revolution of myelin evolution: from reducing metabolic stress to increasing conduction velocity

Excitable cells promote communication within the organism. As species moved from aquatic to terrestrial environments, and their size increased, the distances for nervous connections to reach expanded. To maintain the functional benefit of such nervous connectivity providing fast responses and signals, the evolutionary pressure for fast conduction velocity was introduced. The independent but homologous biological answer is myelin, which first evolved 488 million years ago in the Paleozoic Era (Bullock *et al.*, 1984). Myelin is a fatty acid sheath formed by oligodendrocyte (central nervous system) and Schwann (peripheral nervous system) cells wrapping layers of this substance around the axon. Myelin decreases the membrane capacitance, i.e. reduces the time constant for membrane 'charging' by the amount of current input required to cause a depolarisation. The most advantageous myelin thickness is determined by the biological g-ratio of myelin wraps per axon diameter (Waxman, 1980). Teleost fish optic nerve development comprises a perfect compensation for increased nerve length with increased myelin thickness, the evolution of which could have been driven to maintain the timing of visual information reaching the brain via increasing conduction velocity (Bakken & Stevens, 2012). In early nerve development, these axons exhibit an increase in diameter proportional to their length which increases with age and the size of the fish; the consequences of increased diameter on conduction velocity are explored in the next section.

Although myelin is effective at increasing the speed of conduction, it has been proposed to have first evolved to reduce the metabolic cost of firing action potentials (Crotty *et al.*, 2006). Unmyelinated axons, such as the squid giant axon, rely on propagation and ion flux along the entire axon, conferring a high metabolic demand for ion equilibration by the Na/K pumps. Myelin increases resistance only in areas where it is present, promoting saltatory conduction where ionic currents 'shunt' along the axon, jumping between the nodes of Ranvier. Therefore equilibration and homeostasis of ionic gradients only occurs at the nodes, affecting the distribution of membrane channels and pumps to the nodes, and reducing overall energy requirements from the cell. Stiefel and colleagues (2013) support the hypothesis that the primary role of myelin changed from reducing metabolic requirement in association with the resulting effects of the end-Permian extinction event that created an environment of increased predation, necessitating increased conduction velocity for 'performance enhancement' in predator-prey interactions (Vermeij, 1987; Stiefel *et al.*, 2013). This period is also referred to as the 'Mesozoic Marine Revolution', and it is during this time, 100-160 million years ago, that many

species divergences occurred, such as the cephalopod lineage splitting, separating squid, cuttlefish, and octopus (Tanner *et al.*, 2017).

The structure of the node still holds an aura of mystery, with new genetic and visualisation analysis uncovering locations and distributions of ion channels that appear incongruous with current theories of action potential propagation. The most prominent ion channel in the mammalian node of Ranvier is the $Na_V1.6$ channel, a voltage gated sodium channel that facilitates inward sodium flux during the action potential. The density of $Na_V1.6$ in the node of myelinated axons is the highest in the brain, between 1000 - 1400 channels per μm^2 (Neumcke & Stämpfli, 1982). Potassium selective ion channels of the two-pore domain (K2P) are present in the nodes (Maingret *et al.*, 2000). K2P type channels act to maintain a negative membrane potential through facilitating potassium leak flux out of the axon; enabling appropriate activation of sodium channels in the action potential and aiding membrane repolarisation (Schwarz, 2021). K_V7 channels are highly present in the node, and contribute to the resting membrane potential (Schwarz *et al.*, 2006); this negative membrane potential affects sodium channel inactivation, explored in Section 3.2. Whilst $K_V7.2$ channels are present in large-diameter, $K_V7.2$ and 7.3 present in small and intermediate diameter axons, though the reason why remains unknown (Schwarz, 2021). Mitochondria are absent from nodes, instead located between 3 and 4 µm from the centre of the node, shown in mouse and guinea pig (Edgar *et al.*, 2008; Perge *et al.*, 2009).

1.5 Axon diameter affects action potential propagation

It will soon become apparent how pertinent the mouse optic nerve is as a model for central white matter tracts in electrophysiology research. This nerve contains approximately 25,000 axons from retinal ganglion neurons, and in *ex vivo* nerve experiments lacks synapses, so extracellular nerve recordings present cumulative traces referred to as the CAP (Allen *et al.*, 2006; Brown *et al.*, 2003). An interesting phenomena lies in the distribution of axon diameters, because axon size has not been driven to reach the same optimal diameter. The distribution of axons is not explained by developmental processes with the axons starting small before maturing to the larger axon sizes. Mammalian optic nerves have been studied and show similar axon size distributions. In tree shrews, distribution was measured to be 10% large (1.39 µm), 20% medium (0.88 µm), and 70% small (0.55 µm) (Drenhaus *et al.*, 1997). Cat optic nerve axon distribution is 5% large, 55% medium, and 40% small diameter (Williams & Chalupa, 1983). This skewed distribution towards smaller axon sizes is present across optic nerve or equivalent tracts in the species depicted in Figure 3: mouse, octopus, monkey, human, tree shrew, and guinea pig (Honjin *et al.*, 1977; Camm, 1986; Sanchez *et al.*, 1986; Mikelberg *et al.*, 1989; Drenhaus *et al.*, 1997; Perge *et al.*, 2009).

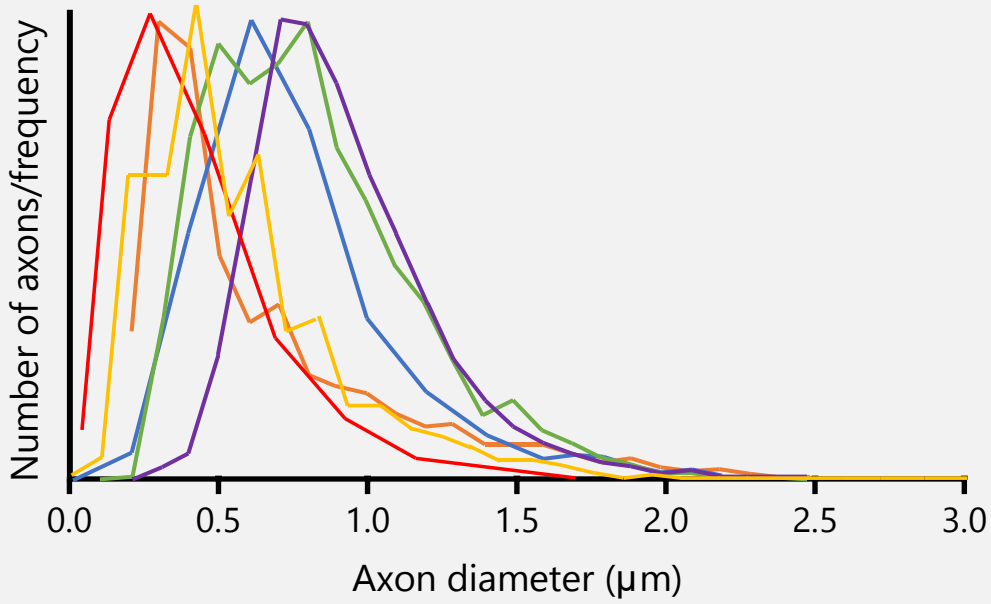

Figure 3. Evolutionary conservation of axon diameter distribution in optic nerve, replotted from six studies. Octopus (red, (Camm, 1986)), human (orange, (Mikelberg *et al.*, 1989)), tree shrew (yellow, (Drenhaus *et al.*, 1997)), monkey (green, (Sanchez *et al.*, 1986)), mouse (blue, (Honjin *et al.*, 1977)), and guinea pig (purple, (Perge *et al.*, 2009)). The y-axis represents the number of axons and frequency normalised to the peak, to account for the differences in data collection. (Data recapitulated from the references by the author).

Octopus tracts to the chromatophore lobe present the same diameter frequency distribution as chordate optic nerve (Camm, 1986). Given that the common ancestor for all these species was likely a flatworm 750 million years ago (refer to Figure 1), the conserved presence of the small-diameter skewed distribution indicates a positive selection pressure for axon diameter. As with many evolutionary pressures, a functional benefit is often the leading cause. Research of cat visual systems investigated the distributions of axons, and correlated these relative populations of axon diameters with the classes of retinal ganglion cells: tracts to W- X- and Y-ganglia have separate functional roles, such as excitation from different retinal pigment cells, detection of movement or light intensity, and having transient or sustained responses (Williams & Chalupa, 1983). These cell-types have different physiological roles in sight and have different diameters to support these roles. Apparent functional homologs exist in the tree shrew and through electrophysiological classification of the dorsolateral geniculate nucleus of owl monkey (Sherman *et al.*, 1975; Williams & Chalupa, 1983). Cross-species similarities in structure supports the valid use of MON as an indicator for processes that can be applied to human physiology.

What is the functional benefit of having axons of different diameters? Increased axon diameter decreases the axoplasmic resistance of the axon, making it 'easier' for ions to move along the axon, therefore conduction velocity increases. Increasing the diameter also increases the

membrane capacitance linearly, however the squared-radius relationship formed from axoplasmic resistance has a larger effect on the conduction (Eq. 4).

$$\Delta V = \frac{1}{r_i c_m} \quad \text{Eq. 4}$$

where ΔV is the change in voltage of the membrane, r_i is the internal axoplasmic resistance (Ohms per cm), and c_m is the membrane capacitance of a 1 cm length of axon. In the Mesozoic Marine Revolution, the increased overlap in species habitats and food sources introduced an increased competition between predators and prey, promoting mechanisms for fast nerve conduction velocity. The giant squid axons are accepted to have been formed via this selection pressure, to maximise the escape reflex of the species through fast-synchronous contractions of the mantle.

Interspecies application of data is valid in the same nerve-type, e.g. the optic nerve, however intraspecies comparison of nerves is more challenging. Take the mouse optic and sciatic nerves as an example. The sciatic is a vertebrate-peripheral nerve tract made up of sensory and motor neurons. This nerve contains a mixture of myelinated α and β fibres, and clumps of small unmyelinated c-fibres, which provides many challenges when attempting to compare electrophysiological responses. The sciatic nerve is the longest in the body which likely compensates for the long distance required to convey signals from foot to the spinal cord. On the other hand, the optic nerve is present on the cranium therefore the length and diameter have no requirement to be long or large because the short distance makes a negligible contribution to reducing conduction velocity. This highlights the interesting axon distribution in the MON, because although small axons contribute the most, a population of large axons are also present (Perge *et al.*, 2009). The assumed reason for large axons has been to increase conduction velocity, but when this need is not required is there another driving force for large axon diameter? Some biological networks incorporate 'neuronal conditioning', where a neuron primes a post-synaptic cell, altering the neuronal response to future signals from other pre-synaptic cells. The monosynaptic pathways of the visual system from cone and rod cells to the visual cortices would not require such processing, therefore this would not explain larger axons having quicker signals to prime cellular responses to the small axons (Perge *et al.*, 2012).

Myelin evolved to reduce the metabolic demand on neurons prior to being selected as a mechanism with the benefit of increasing conduction velocity. Have MON large axons been evolutionarily conserved to combat a high metabolic demand? Perge *et al.* (2012), explored this question hoping to understand the reason for differing axon 'calibre' in terms of the information transferred by each axon, and the functional capacity that links diameter with metabolic resilience. Mitochondria are organelles that hugely determine the cell's metabolic capacity, present in the axoplasm of neurons. In optic nerve axons, the mitochondrial volume increases with respect to axon diameter in a squared relationship (Perge *et al.*, 2009). The frequency distribution of axon diameter was found to correlate with the mean firing rate indicating that larger axons could cope with a high firing rate (Perge *et al.*, 2009). The authors proposed that most information in the guinea pig optic nerve is transmitted at a low rate in the thin axons. Koch and colleagues used multi-electrode arrays to determine how much information the human retina sends, calculating a mean rate of between 6 and 13 bits per

second per cell (Koch *et al.*, 2006). Note that the rate of data transmission of the retina, when all ganglion cell transmission is accounted for, is approximately the same as an Ethernet! The metabolic requirement of an axon changes depending upon the firing rate, which is a factor related to diameter. Doubling the bit-size transmitted requires a 2.6 fold increase in mitochondrial volume to supply the axon with adequate energy to maintain action potential propagation as determined through Eq. 5 (Perge *et al.*, 2009). In optic nerve, small axon diameters present the optimal pay-off between firing at a high frequency and not exacerbating the metabolic capacity of the cell: compare Figure 3 for the most frequent axon diameter in guinea pig, and Figure 4 for the optimal diameter for metabolic capacity to conclude that these both lie at around 0.7 µm (Perge *et al.*, 2009).

$$E = Volume_m + basal\ costs \qquad \text{Eq. 5}$$

where E is the total cost, $Volume_m$ is the volume required by mitochondria, and the basal costs are in units of mitochondrial volume per axon length in μm^3.

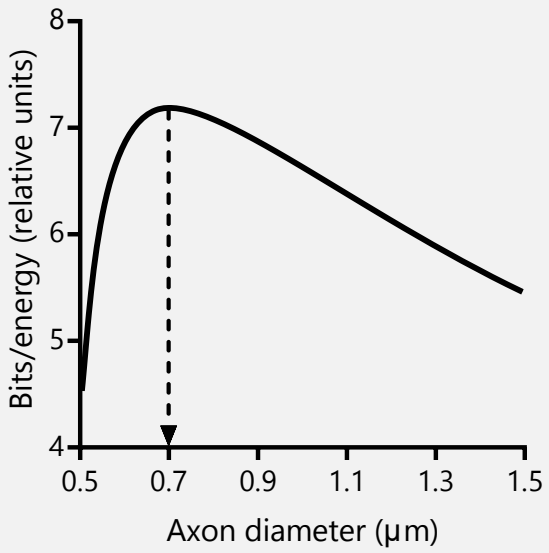

Figure 4. The optimal diameter for bits per energy cost lies around the most frequent axon diameters in guinea pig; 0.7 µm (indicated by a dashed line), shown in Figure 3. Data replotted using Eq. 5, from (Perge *et al.*, 2009).

Bit size is a hard factor to measure in physiology, therefore firing rate is often modelled instead, utilising frequencies that have been recorded in physiology e.g. optic nerve axons fire between 1 and 100 Hz, with the basal rate lying between 5 and 10 Hz (Koch *et al.*, 2006). Thick cochlea axons have been recorded to fire at up to 140 Hz, with a diameter distribution peak at 1.9 µm (Gleich & Wilson, 1993; Merchan-Perez & Liberman, 1996). This diameter is significantly different to optic nerve, highlighting the intraspecies differences in nerves. However, it also supports the electrophysiological use of stimulation frequencies at these levels, as the axons should have the underlying mechanisms to cope with brief stimulation.

Due to the intense metabolic requirement of neurons, this research suggests that the evolutionary drive for axon diameter could sustain firing in intense situations, to retain functional propagation.

1.6 Metabolic explanation for large axons

The squid axon model is obsolete for application to human physiology for a few reasons. First, the lack of myelin would have required a higher metabolic cost as equilibration of ion gradients would have occurred along the entire axon length. Second, squid have an extra external membrane forming a small volume around the axon, which alters the continuity of ions moving between the axon and the bathing solution due to the relative membrane impermeability (Frankenhaeuser & Hodgkin, 1956). Third, being a singular axon rather than thousands packaged in a nerve could also affect the physiological responses: particularly as squid giant axons have no astrocytes in the surrounding area. Mammalian axon firing is followed by a transient increase in the interstitial potassium concentration, which is spatially buffered by astrocytes (Kuffler *et al.*, 1966). These glial cells are connected by gap-junctions, forming a syncytium, thus enabling a wave of membrane depolarisation to travel from the nodal regions of high-activity axons, to distant areas of the nerve under low-activity (Orkand, 1986; Giaume *et al.*, 2010). This occurs because the astrocyte membrane potential is solely determined by the extracellular potassium concentration ($[K^+]_o$), responding in a manner predicted by the Nernst equation (Kuffler *et al.*, 1966). As $[K^+]_o$ increases, the astrocyte membrane depolarises (shifting towards E_K), producing a voltage gradient that determines an influx of potassium ions. The wave of depolarisation passes through the syncytium until in distant regions the membrane potential is more depolarised than E_K and potassium efflux from the astrocyte occurs (see Hopper *et al.*, 2022, Figure 4). This mechanism prevents large increases in $[K^+]_o$ which could affect nerve function. Fourth, in the experiments conducted by Hodgkin and Huxley, the requirement for energy substrates in the artificial cerebrospinal fluid (haemolymph, sea water) was not understood, and therefore preparations would have been negatively affected, particularly in models of metabolic challenge. Brown *et al.* (2003) showed that MON sustains optimal firing for up to 17 minutes before the CAP falls in the presence of zero glucose, however as is described by the authors, these axons have an astrocytic glycogen supply that provides an additional energy source not present in squid. Nowadays the MON has become the gold-standard, with *ex vivo* electrophysiology a useful method to test the effect of metabolic insults like hypoglycaemia, or metabolic challenges like high frequency firing on the CAP (Brown *et al.*, 2003; Allen *et al.*, 2006; James *et al.*, 2010). The main advantage of using high frequency stimulation, is that this retains the physiological environment, but utilises the innate properties of the axons in the nerve to respond as they would *in vivo*. This is why high frequency is used as a metabolic *challenge,* rather than insults like removing substrates from aCSF, to describe this recoverable stimulus.

Overlooking the limitations of the model in question, the squid giant axon still provides a wealth of information in regards to the function, and dysfunction, of the action potential. Hodgkin and Katz (1949) were interested in the all-or-nothing response of the action potential, and experimented with the initial sodium-driven depolarisation phase to alter the peak amplitude of this process. Taking note from their previous works, indirect methods exploiting

the Nernst equation were applied to the experiments. Reducing the extracellular sodium concentration ($[Na^+]_o$) in the sea water bathing solution of the squid axon caused a predictable decrease in the action potential amplitude based upon the changes in E_{Na} (Hodgkin & Katz, 1949). These experiments show that the action potential is not a fixed profile or response, and can be altered by changes to the ionic gradients governing the flux. Six years later, Hodgkin revisited experiments that focussed on exploring changes to the action potential, with more advanced electrophysiological equipment. The effect of high frequency firing on the action potential was measured using the *ex vivo* squid giant axon preparation. This thesis concluded that it was the build up of extracellular potassium within the small space, only 300 Å, created by the external membrane which reduced the membrane potential and resulted in the action potential peak falling until propagation ceased (Frankenhaeuser & Hodgkin, 1956). Measurements showed that although one action potential could increase $[K^+]_o$ within this space by 1.6 mM, the ions diffused exponentially within 30 – 100 msec (Frankenhaeuser & Hodgkin, 1956). This study showed a direct relationship between $[K^+]_o$ and the functional ability of the axon to propagate action potentials without loss of signal amplitude.

Acknowledging the role of $[K^+]_o$ in squid axon propagation failure, Ransom *et al.* (2000) investigated the effect of $[K^+]_o$ in the MON to determine if the principle physiological cause was the same. Using potassium sensitive microelectrodes, they found that 100 Hz stimulus for 1 and 10 seconds caused the $[K^+]_o$ to increase by approximately 2 and 3 mM respectively (Ransom *et al.*, 2000). Consider the differences in models here to appreciate how low this concentration increase is in MON vs squid. The potassium response to stimulus comprises of a biphasic profile which is underpinned by two time constants: the first fast time constant stage occurs due to glial-removal of potassium in the local area, the second slow time constant represents the potassium released from glia and re-up-taken by the neuronal axons (Ransom *et al.*, 2000). These removal mechanisms utilise the Na/K pumps distributed on both cellular membranes. The Ransom *et al.* (2000) paper describes the after-effects of potassium responses to firing, however it doesn't implicate the high $[K^+]_o$ as a cause of CAP amplitude reduction. Despite the potassium concentration increasing, it is important to note the relative concentrations. A recent study found that CAP reduction of MON following intense firing frequency doesn't increase $[K^+]_o$ above 6 mM (Bay & Butt, 2012). These authors observed the function of the mechanism of potassium regulation through glial inwards rectifying potassium channels (Kir) in MON models. A stimulus from 1 to 35 Hz produced a transient increase in $[K^+]_o$ that correlated to a decay in the CAP (Bay & Butt, 2012). If $[K^+]_o$ does not rise significantly, it is unlikely that potassium is driving the drastic fall in the CAP profile that occurs under high frequency firing. The implication being that another ion is responsible for mammalian action potential propagation reduction.

The early research by Hodgkin and Katz showed that decreases in $[Na^+]_o$ causes the action potential profile to drop, so could this be the mechanism? Intracellular sodium concentration ($[Na^+]_i$) is very low, therefore long stimulation trains of action potentials would introduce a large influx of ions into the axoplasm. Marder and Zang (2021) modelled the negative effect of intense firing ('spiking') on future action potential propagation and the intracellular sodium accumulation in unmyelinated and myelinated neurons. The resulting ion influx from one action potential does not largely increase $[Na^+]_i$, however under firing at higher frequencies

(50 Hz – 60 Hz), the sodium accumulates quickly in the node, altering the E_{Na}, and lowering the proceeding peaks of action potentials (Zang & Marder, 2021). Myelination resulted in the $[Na^+]_i$ increase from one action potential recovering after 0.1 second (hundreds of milliseconds), with the removal mechanism contributed more by diffusion along to the internodal regions than activity of the Na/K pump (see Zang & Marder, 2021, Figure 1C). Relevant to our earlier question concerning the reason for the different diameter axons, this thesis explores the differences diameter has on $[Na^+]_i$ increases. It should be noted that although it is not possible to accurately measure individual axon sizes and the respective responses to high frequency firing, understanding the contribution of axon size to the CAP trace provides a strong indication into the role of diameter (one of the main objectives of this thesis). The model proposed by Zang and Marder predicted that myelinated axons at 1.0 µm diameter would exhibit action potential peak reduction from 60 Hz, whereas 0.2 µm diameter axons fail from ≥ 50 Hz (Zang & Marder, 2021). Large diameter axons have a smaller surface area to volume ratio, thus contain a large volume of axoplasm for sodium ions to diffuse into, expediting sodium removal via membrane-bound proteins. The relationship between surface-bound Na/K pumps and the mitochondria within the axoplasm is directly affected by the axon diameter. Na/K pump and mitochondrial density remains consistent irrespective of axon diameter, however these parameters affect each other. As the surface area doubles, the volume increases as the square of the radius, thus large axons will contain a much higher mitochondrial to Na/K pump ratio, promoting the resilience of large axons to metabolic challenge.

The evolutionary advantage of having cells resilient to different levels of stress is the beneficial pay-off between cell populations that can cope with intense stress, and cells that can confer the highest amount of information per action potential (small axons). In this thesis we aim to investigate the ability of axons in the MON to withstand high frequency firing as our model of metabolic challenge. Using previous electron microscopy recordings that show the MON contains different sized axons, and acknowledging that the CAP has a tri-peak profile, we aim to use electrophysiological experiments to support the natural conclusion that the three peaks correlate to axon diameter. This thesis will use experimental methods to test this conclusion. The MON is an excellent model to study the different responses of axon subpopulations because a controlled protocol can be applied to the axons to test the effect of stimulus frequency (dependent variable) on the CAP and $[K^+]_o$ (independent variables). We will use three main protocols in electrophysiology on the MON: high frequency firing, changing the ionic concentrations in the aCSF, and simultaneously measuring the CAP and $[K^+]_o$. We aim to experimentally explore the cause of the fall in CAP under metabolic challenge, and use this to consolidate the findings by Ransom *et al.* (2000), Bay and Butt (2012) and the model described by Zang and Marder (2021).

The main objectives are as follows: A) to determine if the axon populations respond differently to frequency firing based on diameter, B) to use indirect methods with ion substitutions, particularly for sodium and potassium, to determine the likelihood of each ion contributing to action potential peak reduction, C) implementing potassium sensitive electrodes to directly measure elevations in extracellular potassium and then compare those with experimentally induced changes in aCSF potassium, to explore the concentrations at which the compound action potential fails in mammalian axons.

2 Methods

2.1 Ethical considerations

All experiments conducted in this thesis followed the Animals (Scientific Procedures) Act 1986, and were approved by the University of Nottingham Ethics committee. Appropriate personal, project, and establishment licences were held, supporting the method of Schedule 1 (S1) cervical dislocation. The model system used for this research was the MON, obtained from 4 – 6 week old adult male CD1 mice, from Charles River Laboratories (Margate, UK). The mice were group housed in a 12:12 light-dark cycle at 22 – 23°C, with food and water available *ad libitum.* This research used 68 mice for 101 nerve recordings; each mouse contributed two optic nerves which can be treated as two independent samples (Rich *et al.*, 2020).

2.2 Dissection

Mice were killed using S1 cervical dislocation immediately followed by permanent cessation of the circulation, through removal of the head. With the mouse head facing away, a scalpel was used to expose the skull from nose to the neck. The optic nerves were cut at the proximal end by the eyeballs, as close as possible to retain the length between 5 and 7 mm. The skull was cut longitudinally from the cerebellum to the nose, with small perpendicular lateral cuts out from this line facilitating the removal of bone to uncover the brain (see Figure 5). The brain was removed from the skull using forceps inserted horizontally into the cerebral hemispheres, flipping the brain 180° maintaining contact at the cerebellar end. The two optic nerves now visible on top, were dissected at the distal end just before the optic chiasm, removing them from the dural sheaths in the process. The nerves were then immediately placed in an interface perfusion chamber (Medical Systems, Greenvale, NY, U.S.A).

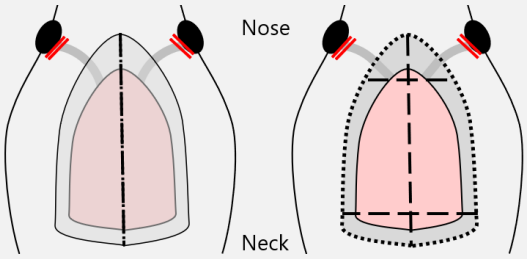

Figure 5. Initial steps in mouse optic nerve dissection. Skull (grey) was exposed in a longitunal slice from nose to neck (dotted line). Optic nerve cut proximally at eyeball with sharp scissors (red lines). Skull removed to expose the cerebrum (pink) through five cuts (dashed lines), starting with the longitunal line followed by outward horizonal cuts.

2.3 Experimental set-up

The set-up is depicted by Figures 6 and 7. MON in the chamber were maintained at 37°C using a TC-202A bipolar temperature controller (Digitimer, Welwyn Garden City, UK). A humidified gas mixture (95% O_2: 5% CO_2) was released from the chamber to flow over the nerve, ensuring the MON was oxygenated. The bathing aCSF was oxygenated with the same composition of gas which maintains the pH at 7.45. The aCSF was made up of a variety of physiologically relevant ions and energy substrates (in mM): 153 Na^+, 3 K^+, 2 Mg^{2+}, 2 Ca^{2+}, 143 Cl^-, 26 HCO_3^-, 1.25 HPO_4^{2-}, and 10 glucose.

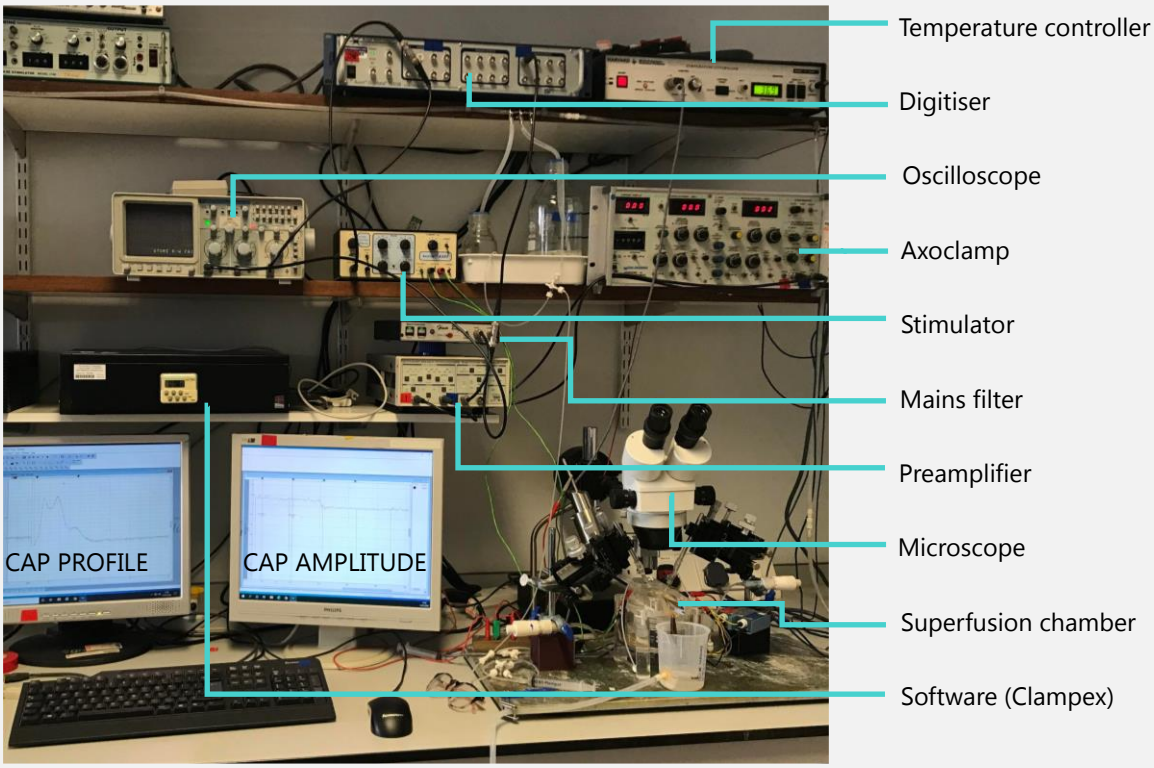

Figure 6. Electrophysiological set-up for conducting high frequency experiments to record the compound action potential of mouse optic nerve. Labelled are the main pieces of equipment used. Note also the jars of aCSF or ion-change aCSF, the piping supplying the CO_2/O_2 mixture, and the superfusion chamber set-up (more detail see Figure 7).

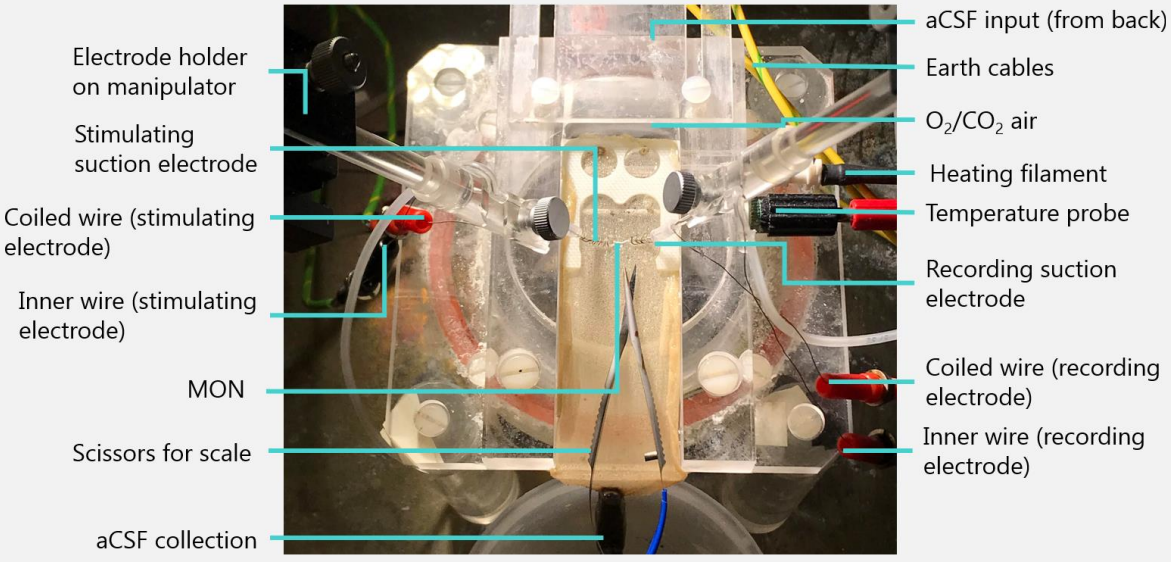

Figure 7. Labelled diagram of the basic experimental set up for mouse optic nerve compound action potential recordings and ion-change protocols. This is a close-up of the basic equipment used to maintain nerve function and conduct a range of experimental protocols.

Suction electrodes were made from filamented borosilicate single barrelled glass capillaries (World Precision Instruments, Sarasota, Florida, USA). The end 5 mm bent by 45^{o} to facilitate placement into the chamber. This end of the electrode was reduced to snugly accommodate the size of the MON, using a Bunsen burner to briefly melt the glass. Two chlorided wires were then attached, with one entering down the capillary lumen and the other coiled around the outside. This process was completed for a second recording electrode. aCSF was backfilled into the electrodes before suction was applied to 'suck up' the nerve into each electrode, ensuring that the electrodes are close enough together that the MON was not stretched or taut as this has been shown to alter conduction. The proximally attached electrode stimulated the MON using a 30 μs supramaximal stimulus (125%) that varied per MON; the tighter the fit between nerve and proximal electrode, the smaller the stimulus required to recruit all the axons, as less shunting of signal occurs. The distal electrode recorded the raw CAP trace before sending the signal through the SR560 low noise preamplifier (Stanford Research Systems, Sunnyvale, CA 94089, USA), to amplify the signal up to 1000x and filter at 30 kHz. The reference signal from the coiled wire was subtracted from the main electrode to remove localised interference. 50 Hz mains current was removed with a HumBug Noise Eliminator (Digitimer Ltd, Welwyn Garden City, UK). The desired signal was acquired using an Axon Digidata 1550B running with Clampex 11.3 (Molecular Devices Ltd, Wokingham, Berkshire, UK). The CAP was visualised on the computer using Clampex 11.3.

The control protocol had the MON bathed in aCSF, stimulated at 1 Hz using the Isostim A320 constant current stimulator (WPI, Sarasota, FL, U.S.A.). Before experiments were started, nerves were left for a minimum of 30 minutes to equilibrate. CAPs were averaged every 10 seconds inclusive of all CAP recordings, e.g. a 2 minute duration of 1 Hz was made up of 12 sequential episodes of 10 seconds. In high frequency protocols, the increased frequency was applied in consecutive episodes of 10 seconds stimulus. In reduced sodium experiments where $[Na^{+}]_{o}$ was reduced, an equimolar choline-chloride concentration was added to the aCSF to maintain osmolarity. For similar reasons, in potassium experiments where $[K^{+}]_{o}$ was increased, an equimolar sodium concentration was removed from the aCSF.

2.4 Potassium microelectrodes

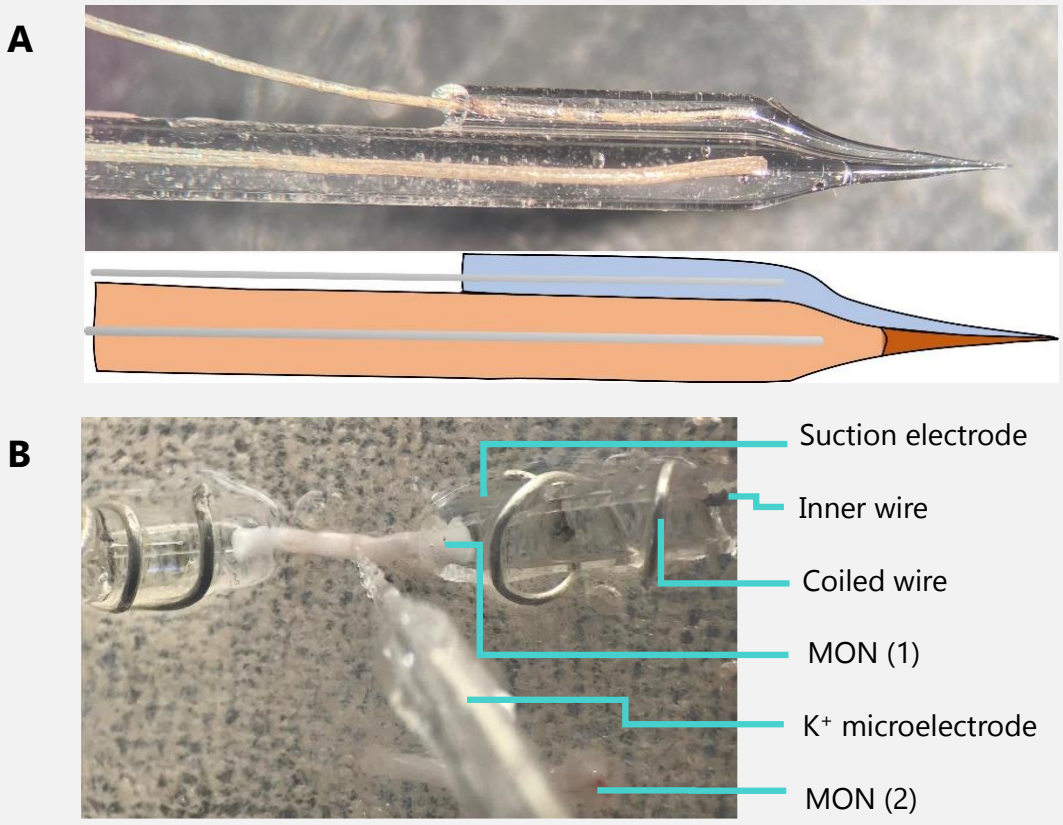

Figure 8. Potassium microelectrode structure. **A.** Photograph (top) and recreation image (bottom) showing a K^+ microelectrode. Note the different sized glass barrels (and electrode wire diameters), and the presence of the meniscus (brown) on the ion-sensitive electrode only, which represents the potassium ionophore. The electrode wires are placed to the same relative point. (Made by the author). **B.** Closeup photograph of the MON attached between two suction electrodes, stimulating (left) and recording (right), with a potassium microelectrode impaling the nerve (bottom). Note the other MON under the potassium electrode.

Manufacture of the electrodes

Potassium (K^+) microelectrodes (Figure 8A) were made from piggyback double barrelled glass (WPI, PB150F-6), following slight modifications to the protocol by Borrelli (1985). The larger glass barrel was the ion-sensitive electrode, and the smaller barrel was the reference (indifferent) electrode, which was broken back to be a third of the length of the larger barrel to fit the electrode holder. Following the glass being pulled to a fine tip using an electrode puller (Narishige, PB-7), the ion-sensitive barrel was backfilled with ~0.5 mm N,N-dimethyltrimethylsilyamine (41716; SigmaAldrich, Merck Life Science UK Ltd, Gillingham, Dorset, UK) and baked for 40 minutes at 180° in an oven (Ambiano mini oven, Aldi). For ease of implementation into the electrode holder, the electrode base was briefly melted using a Bunsen burner. The barrels were then backfilled with different solutions, following the protocol by (Ransom *et al.*, 2000). The indifferent was filled using 34 gauge microfilaments (WPI) with

150 mM NaCl and 20 mM HEPES, pH adjusted to 7.4 using 1 M NaOH. The ion-sensitive barrel was filled using 28 gauge microfilaments (WPI) with 100 mM KCl and 20 mM HEPES, pH adjusted to 7.2 with 1 M NaOH. Under a light microscope (x10), the ends were broken back through manual agitation against a scalpel blade to a tip diameter of ~ 5 µm; using positive pressure (syringe) on the end of the ion-sensitive barrel to ensure no air bubbles were present and that solution could move out the tip. This barrel was then front-filled by suction with K^+ sensitive ion sensor (K ionophore I Cocktail B, 99373, SigmaAldrich), standardised by a column of resin between 100 – 400 µm from the electrode tip. Once filled, these electrodes generally last 24 – 72 hours, provided no air bubbles are introduced between the ionophore resin and solution in the ion-sensitive barrel upon refilling. Without solution, these electrodes could last weeks in air-tight conditions.

Implementation

The K^+ microelectrodes were placed into an electrode holder containing two chlorided silver wires. The first wire entered the ion-sensitive electrode and was attached to an HS-2 x0.0001 MU head-stage which connects to an Axoprobe 1B amplifier. The second wire entered the indifferent electrode and was connected via an HS-2A x0.1 LU head-stage. The signal from the indifferent electrode was subtracted from the ion-sensitive signal, amplified by x10, and passed through a Humbug Noise Eliminator (Digitimer Ltd, Welwyn Garden City, UK) to remove interference from the mains electricity at 50 Hz. A MiniDigi 1A using Axoscope 11 (Molecular Devices) acquired the useful potassium signal at 10 Hz. Following calibration (described below), the K+ microelectrodes were inserted into the nerve using a motorised manipulator to aid nerve implementation (EC1 60-0577 control unit with EC1 60-0571 standard motorised control manipulator: Harvard Apparatus). For simultaneous recordings, the MON was first prepared and inserted into the suction electrodes, then the K^+ microelectrode inserted (Figure 8B). These experiments occurred on an isolated air-table under a Faraday cage to minimise electrical interference.

Calibration

To convert the voltage recordings into quantifiable $[K^+]_o$ recordings, the electrodes were three-point calibrated using a solution of 120 mM NaCl and 20 mM HEPES, and 3 mM, 9 mM or 30 mM KCl (Figure 9A). Electrodes were calibrated individually to ensure they were stable, following Nernstian voltage responses when placed in the three concentrations: upon adjusting baseline 3 mM KCl to 0 mV, placing the electrode in 30 mM KCl should show ~ 50 – 60 mV increase, and 9 mM should lie around 20 - 25 mV (Figure 9B). Only electrodes near to this range with stable recordings were used, experiments used in this study range from 48 to 53 mV. Recalibration after each experiment indicated the stability of the experiments, and any changes of more than 5 mV lead to discarding the experiment. The initial and final calibrations were averaged. The voltage responses were converted into the $[K^+]_o$ using the following Nernst equation rearrangement (Eq. 6):

$$E_k = 61.5\,.\,log_{10}\left(\frac{[K^+]_o}{[K^+]_i}\right)$$

$$V = slope\,.\ log_{10}\left(\frac{[K^+]_o}{baseline}\right)$$

$$[K^+]_o = baseline\,.\,10^{\left(\frac{V}{slope}\right)} \qquad \text{Eq. 6}$$

where V is the differential output from the amplifier (in mV), $slope$ is the electrode response from 3 mM to 30 mM KCl calibration. $Baseline$ refers to the 3 mM potassium concentration in the aCSF, and $[K^+]_o$ refers to the new potassium concentration recorded following the high frequency stimulation. For example, using the calibration from Figure 9B, a 10 mV electrode response would indicate the potassium concentration is $4.65\ mM = \ 3\,.\,10^{\left(\frac{10}{52.95}\right)}$.

The importance of calibration is graphically exhibited in Figure 9C and D, with the exponential $[K^+]_o$ response to increasing voltages shown. The coloured lines represent how calibration of the electrodes determines accurate recording of the $[K^+]_o$. As the relationship shifts from 45 mV (green) towards more Nernstian calibrations (61.5 mV in blue), the actual $[K^+]_o$ decreases with the same voltage recorded from the K^+ microelectrodes. This means that were poor quality electrodes to be used, the measurements of $[K^+]_o$ following high frequency stimulation would be exaggerated and larger than physiologically present (Figure 9).

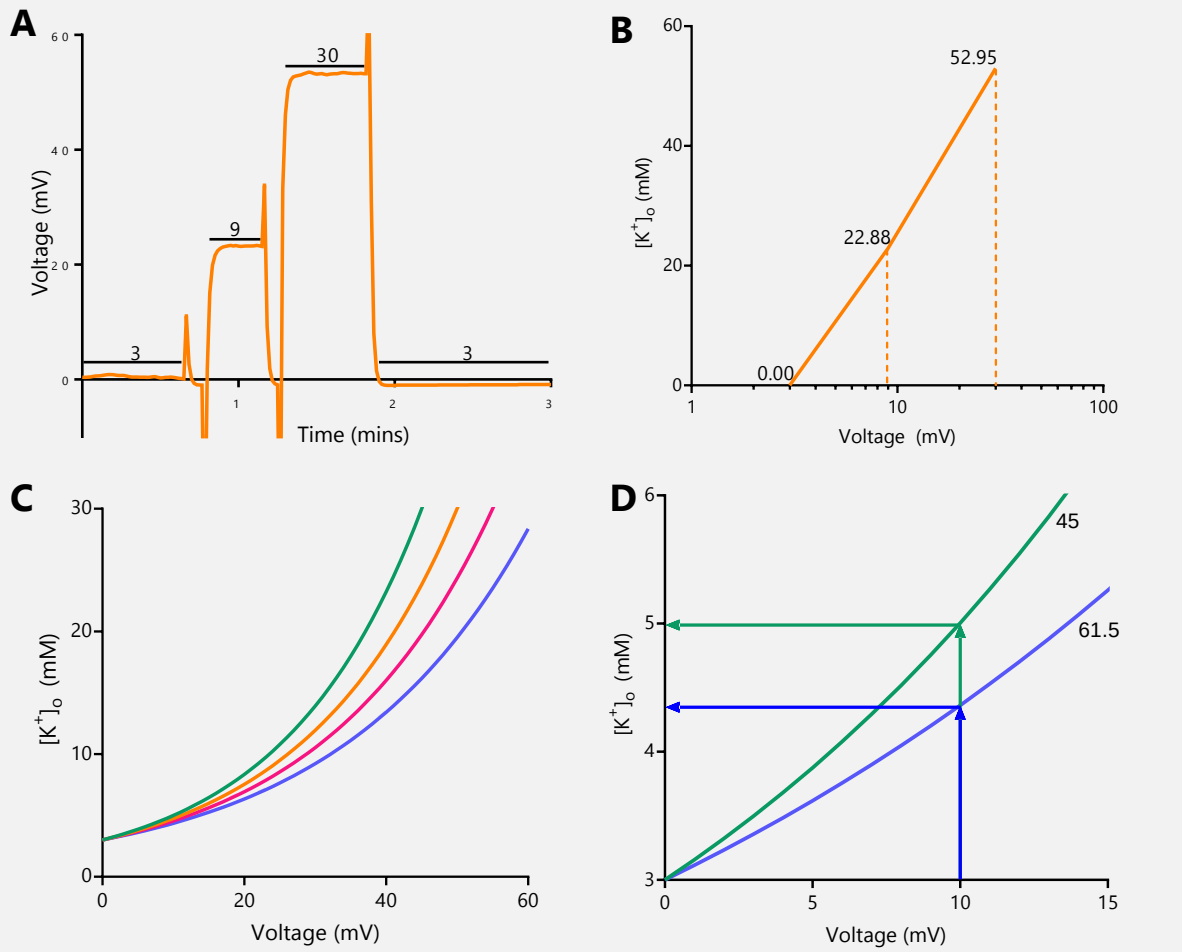

Figure 9. Potassium microelectrode calibration. **A**. Example trace from a potassium microelectrode calibration in 3, 9, and 30 mM KCl (n=1). **B.** Calibration for part A, showing a logarithmic response of the extracellular potassium concentration ($[K^+]_o$) with voltage, with the calibration reaching 52.9 mV, an acceptable experimental magnitude. **C.** Modelled calibrations for the voltage changes plotted as $[K^+]_o$, showing how the calibration can affect accurately recording $[K^+]_o$ as the decade voltage change increases from 45 mV (green), 50 mV (yellow), 55 mV (pink), to the Nernstian 61.5 mV (blue). **D.** Highlighting the importance of calibration: a 10 mV response of the potassium microelectrode could equate to a $[K^+]_o$ of 4.25 mM (61.5 mV calibration, blue), or 5 mM (45 mV calibration, green).

2.5 Data analysis

The calibrations of potassium microelectrodes and the post-experimental data manipulations were conducted in Microsoft Excel (Microsoft), and presented in GraphPad Prism 9.3 (Dotmatics). Analysis of the tri-peak CAP was conducted using Clampfit 10.4 and 11.2 (Molecular Devices), followed by data manipulation and conversion in Microsoft Excel and GraphPad Prism 9.3. Measuring the peak amplitudes was complicated by the interactions between the axon populations because peak 2 (blue dash) superimposes on peak 1, therefore the actual amplitude of peak 1 is smaller than observed (green dash) as the observed peak (black peak 1) contains a considerable contribution of axon responses from peak 2 (Figure 10). The area of peak 1 was measured with a Gaussian fit and converted to the amplitude used,

eliminating interference from peak 2, all conducted using Clampfit. This was conducted based upon Eq. 7:

$$Amplitude = \frac{Area}{(w.\sqrt{\frac{\pi}{2}})} \qquad \text{Eq. 7}$$

where w is the width of the peak. The peak width and peak positions are consistent between MON preparations, it is the peak amplitudes which exhibit variation determined by the dissection and fit of nerve into the suction electrodes. The separation of peak 2 and peak 3 enabled direct measurements of amplitude to be used, as there is no significant overlap and the observed CAP (black) matches with the Gaussian fits (blue and red dash, respectively).

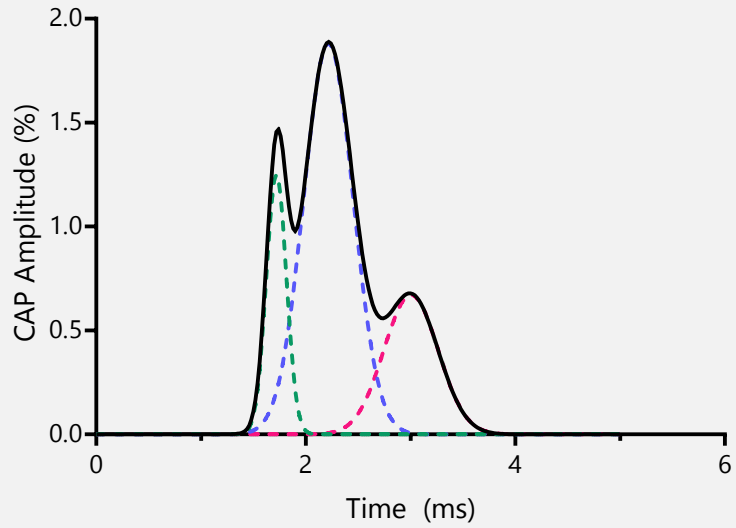

Figure 10. Recording of a MON CAP trace (black) with the stimulus artifact removed and the peaks fitted with three distinct Gaussian distributions using Clampfit: Peak 1 (green), Peak 2 (blue), Peak 3 (red). Note the second peak superimposes on the first, so the amplitude is calculated from the normal-fit rather than the voltage trace.

The CAP amplitude data is normalised to 100% during baseline firing at 1 Hz in control aCSF, to enable comparison of data between MON preparations that have differing absolute voltages, caused by MON fit in the suction electrode affecting stimulus voltages.

The Hodgkin and Katz (1949) paper showed that a reduction in $[Na^+]_o$ caused the action potential amplitude to reduce. Using this relationship, we can predict how the $[Na^+]_i$ changes with high frequency firing, by measuring the CAP amplitude and inputting the data into Eq. 8 and 9. By reducing $[Na^+]_o$, and measuring the CAP amplitudes, we can indirectly quantify $[Na^+]_i$ based upon the peak amplitudes.

Calculating $[Na^+]_i$ from changes to $[Na^+]_o$ requires solving simultaneously the Nernst equation and the logarithmic relationship between CAP change and $[Na^+]_o$ (Figure 15B). CAP needs to be expressed as 100% for the maximum, and we assume $[Na^+]_i$ is 10 mM based on Ransom *et al.* (2000). Rearranging for $[Na^+]_o$ enables the calculation to be solved for E_{Na}, in terms of CAP.

This provides the formula $E_{Na} = 0.57.CAP + 15$, which can be applied to the Nernst equation, re-arranged, and provide the equation to convert recorded CAP peak amplitudes (measured as highlighted previously) into $[Na^+]_i$. The method is described as follows:

Nernst Equation:

$$E_{Na} = 61.5\,.\,log_{10}\left(\frac{[Na^+]_o}{10}\right)$$

$$[Na^+]_o = 10\,.10^{\left(\frac{E_{Na}}{61.5}\right)}$$

Figure 15B Equation:

$$CAP = 46.5\,.\,ln(x) - 133$$

$$CAP = 107\,.\,log_{10}([Na^+]_o) - 133$$

$$[Na^+]_o = 10^{\left(\frac{CAP+133}{107}\right)}$$

Solve simultaneously for E_{Na} with respect to CAP:

$$10.10^{\left(\frac{E_{Na}}{61.5}\right)} = 10^{\left(\frac{CAP+133}{107}\right)}$$

$$10 = 10^{\left(\frac{CAP+133}{107} - \frac{E_{Na}}{61.5}\right)}$$

$$log_{10}10 = \frac{CAP + 133}{107} - \frac{E_{Na}}{61.5}$$

$$E_{Na} = \frac{61.5\,.CAP + 61.5\,.133}{107} - 61.5$$

Main Equations:

$$E_{Na} = 0.57\,.CAP + 15 \qquad \text{Eq. 8}$$

$$[Na^+]_i = \frac{153\,.25}{10^{\left(\frac{E_{Na}}{61.5}\right)}} \qquad \text{Eq. 9}$$

Statistical analyses

The mean ± standard deviation were sufficient for most of the data collected in this thesis as no inferential statistics were required. Throughout the thesis, the n number refers to the number of nerves used per that experimental element, and N refers to the number of nerves used for that figure. Nerves used in the analysis were selected for use provided that the three peaks showed delineation, and the electrical noise was low enough to produce a smooth profile. One-way ANOVA with Tukey's multiple comparisons was applied to the data for Figure 15B to ensure all three peaks followed the same trendline to support the use of the data being averaged and used to underpin the calculations for $[Na^+]_i$ explored above. A sigmoidal dose-response curve was fit to highlight the relationship between increasing $[K^+]_o$ and the CAP amplitude in Figure 16D, to calculate the IC_{50} using GraphPad Prism.

3 Results

3.1 Investigating the tri-peak profile

Supra-maximal stimulation (~125%) of the MON produces a tri-peak CAP profile (Figure 10), consistent across rodent optic nerve models. Previous studies have shown the presence of a range of axon diameters in the MON, thus it could be predicted that the CAP peaks represent three sub-populations of axons distinguished by diameter (Allen *et al.*, 2006). The axon size distribution is plotted in Figure 11A, using data previously collected from electron microscopy imaging of mouse optic nerve. The skewed distribution towards smaller axon diameters is consistent with the six studies of optic nerve data across species shown in Figure 3: octopus, human, tree shrew, monkey, mouse, and guinea pig (Honjin *et al.*, 1977; Camm, 1986; Sanchez *et al.*, 1986; Mikelberg *et al.*, 1989; Drenhaus *et al.*, 1997; Perge *et al.*, 2009).

If one predicts the peaks are contributed to by different axon diameters, two assumptions can be made based on axon physiology: first, the action potentials from large axons will be recorded first since the increase in conduction velocity will decrease the latency of firing, and second, the large axons will be recruited at the smallest stimulus voltages because the smaller surface area to volume ratio will lessen the membrane resistance relative to the squared increase in axoplasmic conductance. Indeed, the three CAP peaks are separated by latency, with the first peak occurring with the shortest latency, then followed by the second, and then with a slight delay the third. This was visualised when noting the final CAP profile in Figure 11B (thick black line). At the lowest stimulus voltages, only the first peak area increased to any measurable value. Upon stimulus increase, the first peak area increased and the second peak started to rise: peak response exhibited in Figure 11B (red line), and the same data plotted as a cumulative distribution in Figure 11C (4 V). At the highest stimulus voltages, the first peak was fully recruited, the second increased gradually, and the third peak increased in a stepwise manner to reach full recruitment.

The CAP area for each peak was calculated and plotted as a cumulative distribution in Figure 11C, using the average from four nerve recordings at increasing stimuli. The maximal stimulus voltage for 11B is 60 V, whilst 11C & D require only 15 V. This occurred because the stimulus experiments were conducted on the same nerves on the same day; nerve diameter varies with age so using litter mate mice of the same age and the same electrodes provides high comparability. The fit of the nerves into the suction electrodes affects the stimulus threshold, i.e. a tight fit of the nerve into the lumen of the electrode requires a smaller stimulus voltage to recruit all the axons as shunting of voltage into the aCSF is limited.

The cumulative distribution plots in Figure 11C provide a mean and standard deviation which, when converted to a classic Gaussian (normal) distribution in Figure 11D, qualitatively produce a peak profile that resembles the experimentally recorded CAP. Figures C and D represent two expressions of the same data, the first as a cumulative distribution and the other as a Gaussian distribution. This links the correlation between stimulus threshold and the three peak distributions, particularly with the spread of data correlating to the CAP profile trace in B. There is a strong correlation between the CAP trace and the stimulus induced normal distribution: first, peak 1 occurs with the shortest latency (large axons have the fastest conduction velocity)

and smallest stimulus threshold (lowest resistance), second, peak 3 is the widest which is reflected in both long latency and highest stimulus threshold.

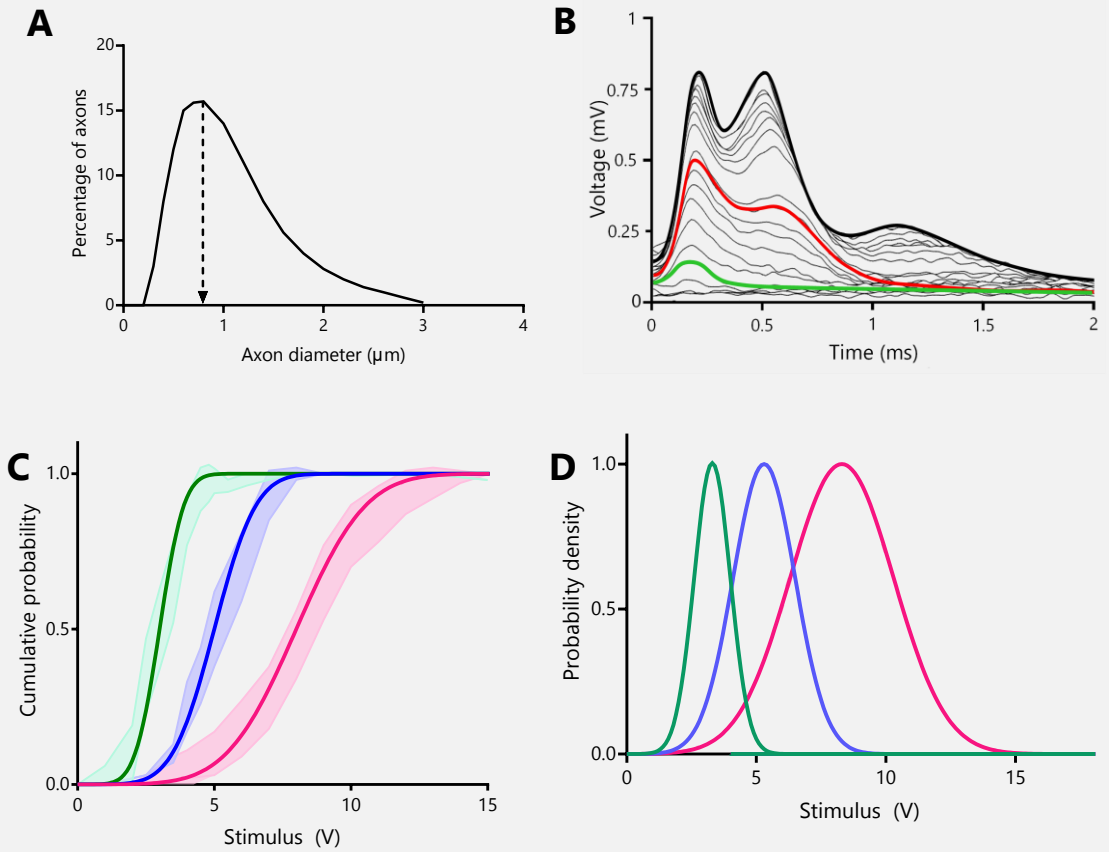

Figure 11. MON has a skewed distribution of axon diameters, and the CAP peaks correspond to axon subpopulations based on diameter. **A.** Frequency distribution of axon diameter. Skewed distribution of axons towards smaller diameters, 0.8 µm has the highest axon percentage indicated by dashed arrow. (Allen *et al.*, 2006). **B**. CAP profile response to increasing stimulus voltage represented as a waterfall plot. Stepwise increase in stimulus voltage from 4 to 60 V leads to an increase in the recruitment of axons, from the first peak to the third peak. Coloured lines indicate example CAP profiles to stimulus voltages, from 8 V recruiting peak 1 (green), 35 V also recruiting peak 2 (red), and 60 V recruiting all peaks (black). Further increases in voltage do not increase the CAP peak amplitudes. (n = 1). **C.** Cumulative probability plot of the differing stimulus thresholds of axon sub-population peak areas in the CAP. Peak 1 (green) is fully recruited over a short stimulus range by 4 V, peak 2 (blue) is fully recruited by 8 V, and peak 3 (red) is fully recruited over the longest range by 15 V. (mean ± SD; n = 4). **D**. Cumulative probability stimulus-threshold effect on the CAP peaks plotted as a Gaussian distribution, with probability density verses stimulus voltage. Note the similarity between this plot and the CAP trace profile in Figure 10. Peak 1 (green) has the smallest recruitment threshold and thinnest spread, followed by peak 2 (blue), and peak 3 (red) with the largest threshold and widest spread.

3.2 Differential sensitivity of the three CAP peaks to metabolic challenge

The main aim of this thesis is to investigate the ways in which the CAP is affected by high frequency firing, and explore possible ionic mechanisms that cause these changes.

Axon potentials have an innate refractory period which is determined by the sodium channel inactivation (absolute refractory period) and changes to potassium conductance across the membrane (relative refractory period). The refractory period of a neuronal action potential is around 20 ms (Hille, 2001). The interval between action potentials is reciprocally related to Hz i.e., 1000 ms in a second divided by the action potential interval (ms) gives the frequency of firing (Hz). Therefore if the given refractory period is 20 ms, this correlates to (1000 ms/ 20 ms) 50 Hz. Using a two-pulse protocol, the CAP fidelity compared to stimulus duration was measured (Figure 12A). The trace insert is used to show the recordings that make up the double-pulse experiment, with the red arrows indicating the increasing stimulus interval from left to right of 4 ms, 12 ms, and 30 ms. This indicates that the change in CAP profile in the other experiments is due to the high frequency stimulation causing a metabolic challenge, as opposed to being an effect due to sodium channel inactivation (I_{Na}). The responses of the three peaks were plotted independently, which shows that the CAP amplitude, although relatively unaffected by 20 ms, significantly reduces when the interval was shortened to 2 ms. The effect is more prominent for Peak 3, where the CAP response reduces from intervals shorter than 20 ms, alluding to the differences in metabolic capacity between the subpopulations which will be highlighted throughout the thesis. Stimuli at 100 Hz (10 ms interval) have a negligible effect upon Peak 1 and 2, with the CAP retaining 90% amplitude between the first and second pulse. Peak 3 shows a response to the short interval, maintaining 75% amplitude. Given this effect, the highest frequency used in this thesis is 100-125 Hz for the CAP; 200 Hz is used to explore the potassium concentration coinciding with frequencies used in previous research (Ransom *et al.*, 2000; Bay & Butt, 2012). Previous research has explored the effect of metabolic insult on total CAP area (Brown *et al.*, 2003), and the change to the tri-peak profile during development (Fern *et al.*, 1998) and myelination (Edgar *et al.*, 2010; Stassart *et al.*, 2018) of MON. Overall, high frequency firing causes the CAP peak profiles to fall (Figure 12). The amount by which the CAP goes down is affected by frequency and duration of stimulus train. Applying varying frequency stimulations at durations of 2, 4, and 5 minutes (longer than the duration used by Ransom *et al.* (2000)), still allows for full CAP recovery. Peak 1 is most resilient to high frequency firing, only dropping by 25% at 90Hz (Figure 12B). In contrast, peak 2 falls by 25% at 45 Hz, and peak 3 at just 11 Hz, highlighting a clear differential sensitivity of the axon-subpopulations to the metabolic challenge. Peak 1 and peak 2 retain full capacity for firing trains of action potentials at the same amplitude between 10 and 20 Hz, the third peak falls in amplitude from 5 Hz. Stasheff (2008) concluded that the optic nerve has an axonal median firing rate of 17.5 Hz, which lies around our average for the first and second peak range for full action potential propagation of the peaks. After 17.5 Hz, the first and second peak fall in a logarithmic relationship with frequency, which appears linear when plotted on a logarithmic scale.

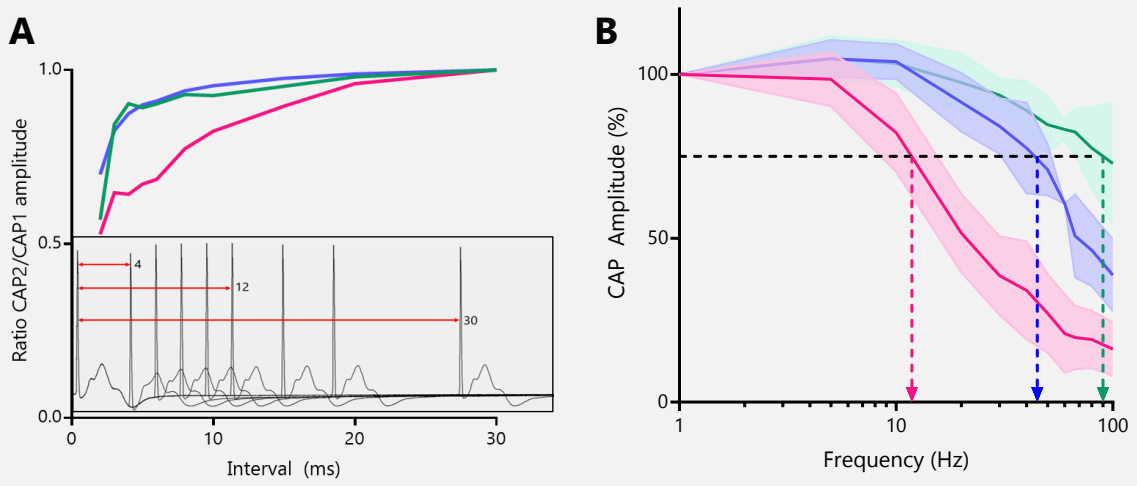

Figure 12. High frequency firing causes the CAP peak amplitudes to reduce**. A**. The effect of stimulation interval on successful action potential production. Peak 1 (green), Peak 2 (blue), and Peak 3 (red). The CAP is affected by intervals lower than 20 ms which correlates to 50 Hz. (n = 1). The double-pulse protocol is depicted in the inset with CAP traces, indicating the response after 4, 12 and 30 ms interval. The vertical spikes are negligible stimulus artifacts. **B**. Differential response of the CAP peaks to high frequency firing. The averaged (mean ± SD) responses of each peak are plotted to show the differing sensitivity of these populations to stimulus frequency at durations of 2, 4 and 5 minutes. Note with frequency plotted on a logarithmic scale, the CAP peak amplitudes fall in a linear relationship. The CAP falls by 25% at 11 Hz for peak 3 (red), 45 Hz for peak 2 (blue), 90 Hz for peak 1 (green). (Peak 1, n = 11; peak 2, n = 12; peak 3, n = 12).

Figure 13A shows the, normalised, traces of two experiments where the frequencies were tested from 5 Hz to 100 Hz for durations of 2 minutes of continuous firing, with at least 4 minutes recovery between stimulations. The experiments were conducted consecutively on the same nerve preparation, (i) first testing low frequencies, then (ii) moving to higher frequencies to test the effect across the whole range. The amplitudes for each peak are shown, in the representative colours of green (peak 1), blue (peak 2), and red (peak 3). Peak 1 is affected the least, and peak 3 affected the most. Observing the shape of the falling phases during stimulation, the amplitude for peak 1 reaches a new plateau within the 4 minutes, indicating a homeostatic re-equilibration and adjustment to the firing frequencies, particularly in 13Ai. In contrast, peak 3 from frequencies ≥15 Hz, does not reach a plateau during stimulation, instead showing the start of an exponential decrease in the amplitude trace. Increased durations of firing were tested later to see if all three peaks reach a plateau, and at most frequencies this does occur, except for the higher frequencies where peaks 2 and 3 fall to zero before reaching a new equilibrium amplitude (data for 20 minute stimulus not shown). It was only after conducting experiments at these smaller durations that we tested larger ones. Previous researchers published using durations of 2 seconds to 2 minutes (Ransom *et al.,* 2000; Bay & Butt, 2012), supporting our decision to use 2 – 5 minutes.

The peak profiles change in two ways when under this metabolic challenge: a) the peak amplitude decreases, b) the rate of rise decreases. This is visualised for peak 2 in Figure 13B where the peak both falls and 'slumps' to the right, as the gradient gets shallower. The effect on the amplitude of the CAP peak 2 can be visualised in Figure 13B through a small change in peak occurring at 40 Hz, however from 50 Hz to 100 Hz the change increases dramatically.

Here we observe that high frequency affects axon subpopulations differently in the nerve, therefore indicating that there is a biological metabolic mechanism that differs as a result of axon diameter. Marder *et al.* (2021), proposed that intracellular sodium ion accumulation positively correlates with stimulation firing frequency, affecting small axon diameters more than larger diameters. Therefore applying this physiological method of metabolic challenge will explore what happens in the MON.

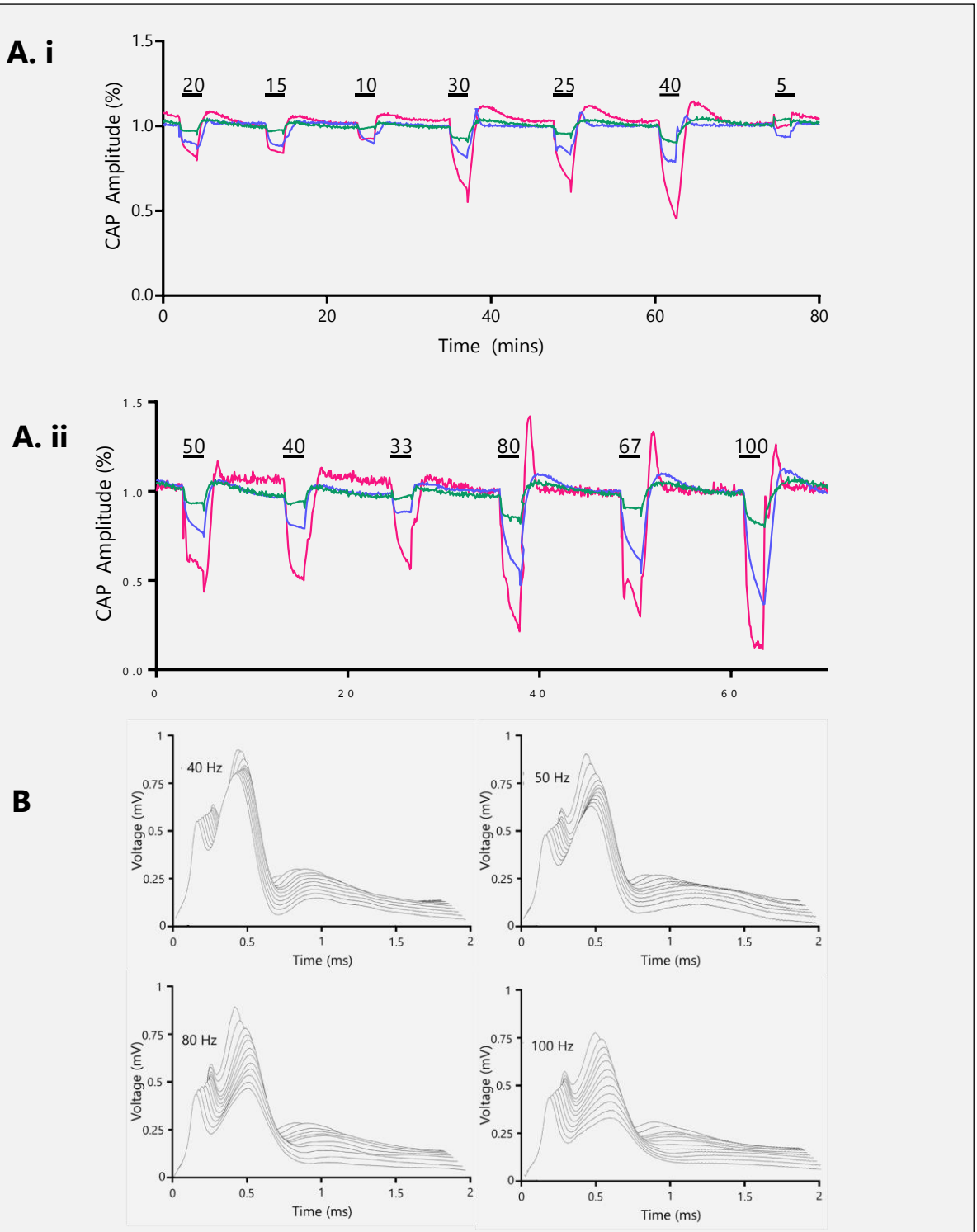

Figure 13. Tri-peak response to varying frequencies, **A. i.** low frequencies from 5 to 40 Hz, **ii.** high frequencies from 25 to 100 Hz. Observing the maximum drop in CAP at 50 Hz shows that peak 3 amplitude falls by 50% whereas peak 1 only drops by 10%. Note the full recovery throughout the experiment with baseline firing at 1 Hz, showing the nerve is capable of recovery after this degree of intense firing. The tested frequencies were stimulated for a 4 minute duration. (n = 1, same nerve preparation). **B**. Waterfall plots of CAP profile response to frequencies stated in each panel. Note the differential fall of peak 3, followed by peak 2, then peak 1. Initial baseline CAP is at the back z-axis, with consecutive traces stacked moving towards the front of the plot during 4 minutes of stimulation.

3.3 Increased $[Na^+]_o$ correlates with a drop in the CAP

Zang and Marder modelled the effect of high frequency firing on action potential fidelity between small, medium, and large axon populations. As we can now directly relate these to the third, second, and first peaks, respectively, our electrophysiological set-up facilitates experimental testing of these hypotheses. It is currently impossible to selectively load axons with a sodium-sensitive dye and the resolution of con-focal microscopy prevents the ability to distinguish two axon diameters e.g. at 0.6 and 0.7 µm. Indirect methods were used given that direct measurements of $[Na^+]_i$ are not possible. Applying the principles adopted from Hodgkin and Huxley, we first evaluated the parameters associated with sodium in the action potential: $[Na^+]_i$ (Eq. 8), $[Na^+]_o$, membrane potential (permeability, conductance), E_{Na} (Eq. 9); these factors can be accounted for in the Nernst equation. The evolutionary success of excitable cells relied upon fine control of the ion gradients, and these same concentrations must be meticulously maintained in MON to retain the action potential peak profile. Therefore, when observing that high frequency firing causes the CAP to change, through reduced amplitude and slower rates of rise of the peak, it is understandable to predict the effect to ionic gradient changes. The low $[Na^+]_i$ means that small increases in sodium influx can have a large effect on the concentration and thus on E_{Na}, particularly in small axons of the third peak where the axoplasmic volume is low.

The indirect method for increasing the $[Na^+]_i$, is to reduce the extracellular concentration by decreasing sodium content in the aCSF bathing the nerve (Figure 14A). This causes a measurable change in the ratios of ion concentrations across the membrane. Thus the CAP amplitude response can be directly related to the ratio of sodium concentrations (Figure 14B). The sodium concentration in control aCSF of mammalian tissues is 153 mM, therefore NaCl was reduced to 100, 80, 60, 50, 40 and 30 mM, with equimolar replacements of choline used to prevent cellular effects confounding the apparent response to sodium. Figure 14B shows that as the $[Na^+]_o$ was reduced, all three peak CAP amplitudes decreased in a logarithmic manner. The exposure durations to low sodium aCSF varied depending upon the time taken for the CAP amplitude to reach a stable plateau, i.e. where the membrane and firing capacity have re-equilibrated to the new ionic concentrations. The CAP tri-peak profile response to low $[Na^+]_o$ and high frequency firing is similar: the peak amplitude reduces and the rate of rise of the peaks decreases. This gives a primary indication that changes to the sodium concentration gradients could have a role in causing the fall in CAP profile in scenarios of high frequency firing.

Figure 14A shows the effect of $[Na^+]_o$ on the second peak, but Figure 14B shows why this is an appropriate representation of the result. The changes in CAP amplitude varies logarithmically with $[Na^+]_o$, in all three peaks. This allows the extrapolation of a line of best fit for the response of CAP amplitude to $[Na^+]_o$: $CAP = 46.5 \ln([Na^+]_o) - 133$ (application of Figure 14B equation). A one-way ANOVA of the averages trends for the three peaks indicates there is no significant variation in the responses, conducting a Tukey's multiple comparison merely confirms there is no significant difference between the responses of P1, P2 and P3 at each sodium concentrations ($p > 0.05$). This supports the use of the average line across the peaks.

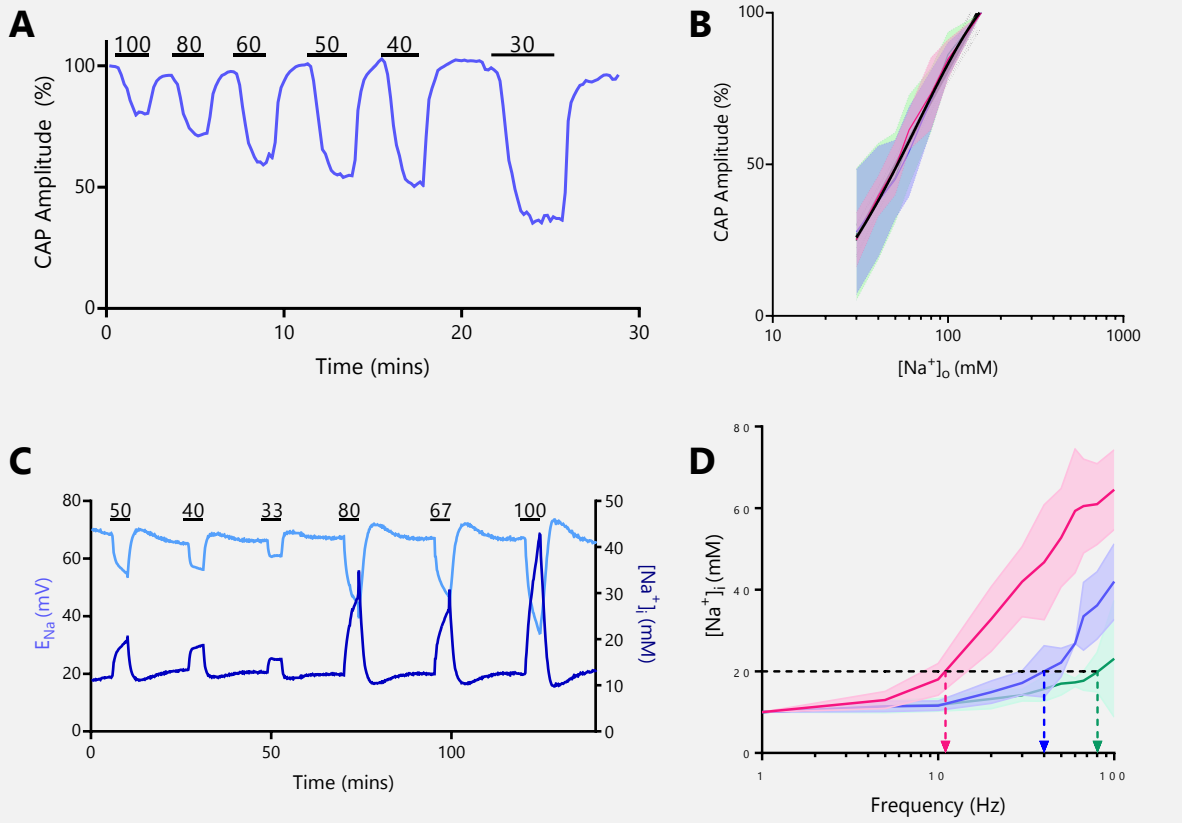

Figure 14. Sodium ion concentration affects axonal action potential peak amplitude. **A.** An example CAP trace of Peak 2 amplitude in response to low $[Na^+]_o$. The aCSF sodium concentrations decreased from aCSF containing 153 mM sodium, to 100, 80, 60, 50, 40, and 30 mM. The nerve was supra-maximally stimulated at 1 Hz throughout. (n = 1). **B**. The logarithmic relationship between extracellular sodium concentration ($[Na^+]_o$) and CAP amplitude. All three peaks respond the same to changes in $[Na^+]_o$. Since the data is plotted on a logarithmic scale, the response can be represented by $y = 46.5\ \ln(x) - 133$ stimulus at 1 Hz was used throughout. (peak 1, n = 17; peak 2, n = 18; peak 3; mean ± SD). (n = 4). **C.** Response of E_{Na} and $[Na^+]_i$ to high frequency firing. The CAP trace from Figure 14C is converted using the Nernst equation and the equation combining extracellular sodium to CAP response in Figure 13B. Note that as the frequency increases, E_{Na} decreases and $[Na^+]_i$ increases. A steady decrease in the E_{Na} coincides with a logarithmic increase in the $[Na^+]_i$. Frequencies tested are 50, 40, 33, 80, 67, and 100 Hz. Stimulus at 1 Hz was used for recovery at baseline (n = 1). **D.** The predicted response of $[Na]_i$ to firing frequency. The averaged (mean ± SD) responses of each peak are plotted to show the differing sensitivity of these populations to stimulus frequency at durations of 2, 4 and 5 minutes. The apparent linear trends indicate that CAP peak amplitudes respond in a logarithmic relationship with frequency. The $[Na]_i$ increases by 10 mM (to 20 mM) by 12 Hz Peak 3, 40 Hz Peak 2, and 80 Hz Peak 1 (Peak 1, n = 11; peak 2, n = 12; peak 3, n = 12).

The logarithmic relationship observed here follows that predicted by the Nernst equation both mathematically and logically. Consider how this formula predicts the E_{Na} which determines the action potential peak amplitude, which is set by the logarithmic ratio between sodium concentrations across the membrane. Applying the simultaneous equations described in the methods, rearranging for the $[Na^+]_o$ when equating this logarithmic equation with the Nernst equation: $E_{Na} = 0.57.CAP + 15$. The amplitude of peak 2 traces can now be interpreted to show the E_{Na} and from this the $[Na^+]_i$ in any experiment using: $[Na^+]_i = \frac{153.25}{10^{\left(\frac{E_{Na}}{61.5}\right)}}$.

The CAP data illustrated in Figure 14C has been processed through these equations to show the effect of high frequency firing on E_{Na} and $[Na^+]_i$. The most interesting point to highlight is that although E_{Na} steadily decreases with frequency of stimulus, the $[Na^+]_i$ remains low at the start, but presents a very large increase when at the smaller $[Na^+]_o$ concentrations. Referring back to the effect of 30 mM $[Na^+]_o$ on the CAP, we observe a fast and significant drop in the profile, like that seen under high frequency firing (Figure 12B). This further supports the effect of CAP drop being a result of increased $[Na^+]_i$ content in the axons.

Previously we determined there is a differential sensitivity of the peaks to high frequency firing. Conversion of the data recorded from these experiments into the relative $[Na^+]_i$ is represented in Figure 14D, where the average response is exhibited as a line and the shaded areas indicate the standard deviation of each peak in response to frequency. Peak 3 (red) is most susceptible to high frequency firing, and likewise shows a logarithmic increase in $[Na^+]_i$. The trajectories of peak 2 and 3 are very similar, both exhibiting a 3.6 fold increase in $[Na^+]_i$ from 10 to 100 Hz (Peak 3: 18 to 64 mM (x 3.6), peak 2: 11.6 to 42 mM (x 3.6), peak 1: 11.8 to 23 mM (x 1.9)). Therefore, despite the different susceptibilities of the three peaks to high frequency firing, once the axon subpopulation starts falling, the rate of increase in $[Na^+]_i$ is consistent between peak 2 and peak 3. Peak 1 is more resilient to high frequency firing up to 100 Hz, with only small increases in $[Na^+]_i$ which is likely due to the increased volume and metabolic capacity of the Na/K pumps to maintain low concentrations. For Figure 14B, the frequency at which all peaks exhibited 75% maximum CAP amplitude is indicated graphically. In Figure 14D, the frequencies at which $[Na^+]_i$ has increased to 20 mM are indicated by the dashed lines and occur at 12 Hz for peak 3, 40 Hz for peak 2, and 80 Hz for peak 1. This is interesting as it suggests that doubling $[Na^+]_i$ correlates to a 25% loss in CAP amplitude. Predictions of the $[Na^+]_i$ concentration response to frequency are related by a logarithmic relationship in the Nernst equation, which accentuates any data points significantly higher or lower than the mean to cause the standard deviations and spread of data in Figure 14D to be larger than Figure 12B.

Here we show that the differential sensitivity of axons could be a result of increasing $[Na]_i$ causing the CAP amplitude to fall, more predominantly in the smaller axons which have a smaller volume. The CAP peak response to high frequency firing (Figure 13A) and the indirect measure of increasing $[Na^+]_i$ by reducing the $[Na^+]_o$ (Figure 14A) shows how the CAP peaks reduce with both of these factors. Visually observing the effect on the tri-peak CAP profile shows how the peaks are affected in similar ways, with the peak and rate of rise decreasing in both experimental protocols.

3.4 Increased $[K^+]_o$ is not the primary cause of CAP amplitude reduction

As alluded to previously, Frankenhaeuser and Hodgkin (1956) concluded that failure of *Loligo* axon conduction was due to $[K^+]_o$ released during the action potentials. Therefore it is pertinent that we assess this variable in mammalian nerve to determine whether accumulation of $[K^+]_o$ could be the cause of CAP amplitudes reducing due to high frequency firing, as opposed to $[Na^+]_i$. Two protocols are used to explore the role of potassium, a) using ion-sensitive microelectrodes to measure $[K^+]_o$ in response to high frequency firing, simultaneously with real time CAP, and b) altering the extracellular potassium concentration and observing the effect on the CAP amplitude and profile.

Previous researchers found that $[K^+]_o$ increases by 3 mM following 10 second stimulus at 100 Hz in rat ON (Ransom *et al.*, 2000), and by 1.6 mM following stimulation in MON (Bay & Butt, 2012). These papers acknowledge the biphasic profile of the potassium concentration during high frequency firing. Ion-sensitive K^+ microelectrodes calibrated using the Nernstian relationship described in the methods, facilitate accurate recordings of $[K^+]_o$ in MON. Likewise, this study records potassium responses that have two peaks, exemplified in Figure 15A with a 50 Hz stimulus for 2 minutes. The letters on the graph correspond to the parameters plotted in Figure 15B. $[K^+]_o$ reaches its maximum (i) within the first 12 seconds in a steep exponential response. This is followed by a slow reduction in $[K^+]_o$, before $[K^+]_o$ increases again to form the second peak phase response. This second peak is driven by the slower time constant of the neuronal release of potassium (Ransom *et al.*, 2000). Rather than drifting back down to baseline following stimulus cessation the potassium shows a prominent, rapidly developing, undershoot (ii) which slowly relaxes towards baseline (iii). The undershoot is explored later on in more detail (see Figure 17).

A comprehensive exploration into the $[K^+]_o$ response is discussed following low frequency firing (1 – 35 Hz) (Bay & Butt, 2012), and short durations at a high frequency (1 to 10 seconds, 100 Hz) (Ransom *et al.*, 2000). This thesis uses longer durations (2 – 5 minutes) at a range of frequencies (1 – 200 Hz) to confirm the $[K^+]_o$ profile (Figure 15A), and importantly measure the absolute increase in concentration (Figure 15Bi) whilst simultaneously recording the CAP amplitude (Figure 16A).

The main parameter we are interested in is the maximal $[K^+]_o$ increase in response to high frequency firing, as this is the factor that Frankenhaeuser and Hodgkin concluded causes the reduction in the action potential peak and profile. Previous papers used frequencies from 1 to 100 Hz for CAP recordings, yet higher frequencies for the $[K^+]_o$ recordings, therefore 200 Hz was used for Figure 15B (and not earlier data such as Figure 14B). 200 Hz is also used in Figure 17C which comprises the same experiments in this figure, alongside the appropriate CAP responses. Figure 15Bi shows that for the same stimulus duration, as the frequency increases, the extracellular potassium concentration increases. With frequency plotted on a logarithmic scale, the resulting effect on $[K^+]_o$ follows a linear pattern, illustrated by the line of best fit on the graph (Figure 15Bi). The maximal recorded increase in $[K^+]_o$ in this study was 1.47 mM, from the baseline of 3 mM, which occurred from 2 minute stimulus at 200 Hz. The magnitude of increase in $[K^+]_o$ is small across stimulations from 1 – 200 Hz, with the mean occurring between 3 and 4 mM across all frequencies. In the same protocol, the MON CAP falls

dramatically (see Figure 13A), indicating that elevated $[K^+]_o$ is not the cause of CAP amplitude reduction. This is because $[K^+]_o$ under high frequency firing (Figure 15Bi) does not increase to a concentration high enough to cause CAP peak amplitude reduction (Figure 16B).

The other two measures stated in Figure 15B describe factors post-stimulus, in the recovery phase. After noting that the potassium increase is followed by an undershoot period, we plotted this concentration against frequency and observe a negative correlation (Figure 15Bii). The amount by which the $[K^+]_o$ drops is determined by the frequency of firing, when plotted on a logarithmic scale. Furthermore, the time taken for $[K^+]_o$ to return back to baseline concentrations (determined by a stable response and flat trend), increases with the frequency firing (Figure 15Biii). This is to be expected as the increased number of action potentials stimulated result in a larger net ion-flow, therefore the ion gradients across the membrane take longer to reinstate.

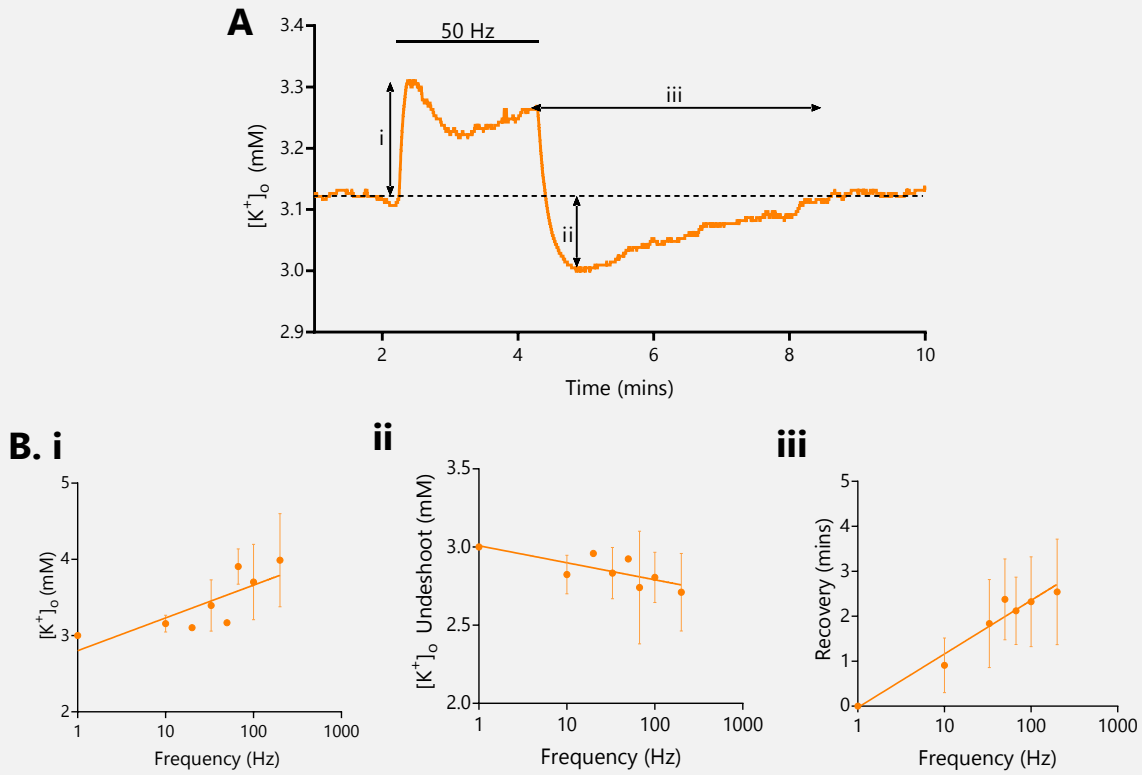

Figure 15. Responses of potassium microelectrodes. **A.** An example trace of the extracellular potassium concentration ($[K^+]_o$) during a 50 Hz stimulus for 2 minutes. Note the concentration increase of 0.2 mM and the biphasic peak response which is explored in detail by Ransom *et al.* (2000). (n = 1). **B.** Semi-log graphs of factors relating to the $[K^+]_o$ profile during and following high frequency stimulus. **i.** Maximum $[K^+]_o$ increases with stimulus frequency, $[K^+]_o$ = 0.19 . ln(Frequency) + 2.8 (mean concentration ± SD, N = 8). **ii.** Magnitude of the $[K^+]_o$ undershoot increases with frequency, $[K^+]_o$ undershoot = -0.05 . ln(Frequency) + 3.03 (mean concentration ± SD, N = 8). **iii.** Recovery time from the maximal undershoot to baseline increases with frequency, recovery time = 0.54 . ln(Frequency) - 0.13 (mean time ± SD, N = 8).

Applying the second potassium experimental protocol indicates the relative nerve CAP responses to changes in $[K^+]_o$ (Figure 16A). Changes to the bathing solution affects all axons the same, due to holistic changes in the relative concentration gradients across the membrane, hence only Peak 2 is plotted in Figure 16A. $[K^+]_o$ was increased from a baseline aCSF of 3 mM up to 9, 10.5, 12, 13.5, 15, and 18 mM, for durations that enabled the CAP to almost reach a new equilibrium at steady-state. Whilst 9 mM only caused the CAP to drop by ~10%, by 12 mM the CAP fell by ~50%, and by 15 mM the CAP failed completely. The nerve was able to fully recover following the administration of normal aCSF bathing solution.

The effect of $[K^+]_o$ on CAP amplitude is best observed when represented as a sigmoidal concentration-response curve, when averaged across four nerves in Figure 16B. The dramatic response of the CAP to potassium concentrations occurs between 9 and 15 mM, with the IC_{50} occurring at 12.3 mM $[K^+]_o$. Due to the natural $[K^+]_o$ in MON occurring at 3 mM, small changes in concentration can have significantly large effects, particularly when acknowledging the Nernst equation. An important factor to note is that despite these concentrations causing the CAP to fall, they are all supra-physiological. Particularly as in the experiments we conducted, all frequencies causing the CAP to fall appeared to have a $[K^+]_o$ that increased no further than 4.5 mM. Based on our concentration curve, 4.5 mM potassium would only reduce the CAP by ~2%, further indicating that elevated $[K^+]_o$ does not directly cause the CAP to drop.

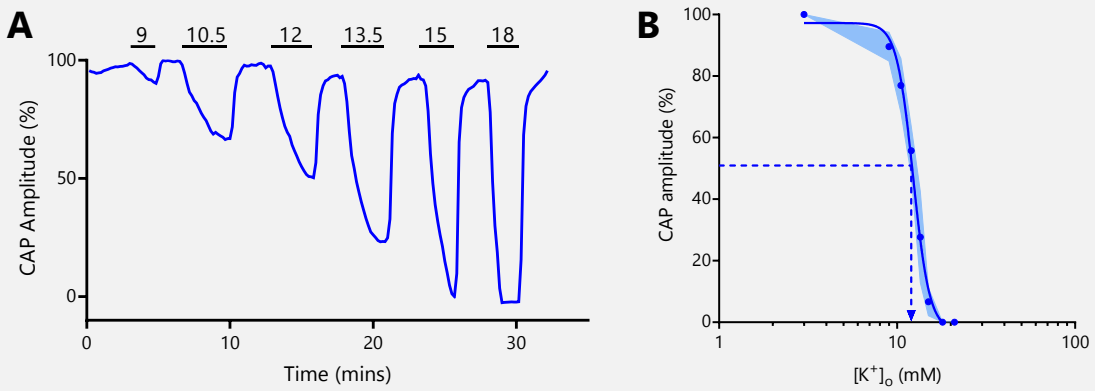

Figure 16. Effect of extracellular potassium concentration ($[K^+]_o$) on CAP peak amplitude. **A.** Peak 2 CAP amplitude reduces in response to high $[K^+]_o$. The aCSF $[K^+]_o$ increased from baseline 3 mM, to 9, 10.5, 12, 13.5, 15, 18 mM. The nerve was supra-maximally stimulated at 1 Hz throughout, (n = 1). **B.** The sigmoidal relationship between extracellular potassium concentration ($[K^+]_o$) and CAP amplitude. Baseline potassium is 3 mM, and the physiological threshold occurs at 9 - 10 mM where any small increase causes a large drop in the CAP and the IC_{50} was 12.3 mM. All three peaks respond the same to the $[K^+]_o$ so average data for peak 2 is plotted for simplicity. Stimulus at 1 Hz was used throughout, (mean ± SD; n = 4).

3.4.1 Correlation between the $[K^+]_o$ undershoot and the CAP overshoot

The methodology utilised enabled concurrent recordings of the $[K^+]_o$ and the CAP amplitude. This protocol is highly technically difficult, leading to a reduced number in total samples and nerve recordings used, however for descriptive purposes this seems sufficient. Furthermore all data collected has the same profile (Ransom *et al.,* 2000) and similar response magnitudes (Bay

& Butt, 2000) to previous studies using rodent optic nerve. If increased $[K^+]_o$ is the primary cause of CAP amplitude drop, one would predict that (**a**) the profile of the response during stimulation should mirror each other, and (**b**) the recovery phases following stimulation should have similar profiles and take the same time to return to baseline. These assumptions can be addressed through observing Figure 17A, which shows an example nerve response to high frequency firing at 50 Hz for 2 minutes. The blue trace (left axis) is the CAP response, and the orange trace (right axis) is the simultaneous $[K^+]_o$ response. This figure shows that although the potassium rises before/in tandem with the fall in CAP during the first 30 seconds of stimulation, the profiles do not continue as mirror images. However, the main assumption (**a**) of having a similar profile does not hold true. The CAP has a steady monophasic exponential falling phase, followed by a recovery phase. The potassium shows a biphasic profile of an initial fast exponential increase, slow recovery, and slower increase in concentration until the stimulus stops. This indicates that there is likely another cause of the CAP peaks to fall: the increasing $[Na^+]_i$ modelled previously and experimentally supported here. Assumption (**b**) poses an interesting consideration. The recovery of both follow an exponential restoration phase where the CAP amplitude increases and the $[K^+]_o$ decreases. However, both phases go beyond the normal homeostatic baseline levels, the CAP amplitude overshoots soon after the $[K^+]_o$ undershoots. Both responses also return back to normal at the same time. This indicates that potassium could have an effect on the recovery phase of the CAP.

In Figure 17A (and 13A) when observing the fall in CAP amplitude as a result of high frequency firing, the profile shows an interesting response. The post-stimulation recovery phase of the CAP peak amplitude shows an overshoot of the baseline, occurring following cessation of high frequency stimulation. The magnitude of the peak amplitude overshoot increases with stimulation frequency. Due to the ease of protocol to change the $[K^+]_o$, we lowered the baseline concentration to 2.5 and 2 mM, and found that the CAP amplitude increased above that at baseline concentration (Figure 16B). The trace exhibited in Figure 17B, shows the resulting effect of reducing the $[K^+]_o$ to 2.5 and 2 mM, followed by a 5 minute stimulation at 100 Hz. Conducting both methods on the same nerve in the same experimental conditions increases the validity of our assumptions, particularly that the CAP overshoot could occur due to a reduction in the $[K^+]_o$.

The $[K^+]_o$ increases in respect to the frequency stimulation. We show earlier that the CAP falls in a linear relationship when the frequency is plotted on a logarithmic scale (Figure 12B), therefore it follows that the CAP varies logarithmically with $[K^+]_o$ too. We previously predicted that the $[Na^+]_i$ increases logarithmically with frequency (with a differential sensitivity to axon diameter determined by the peak sizes), hence the potassium concentration would increase during stimulus-induced action potential efflux of potassium. The effects observed are based upon the cumulative response of axons in the vicinity of the potassium microelectrode, so at higher frequencies, when the third peak axons are unable to fire, the amount of potassium being released from the axons will be reduced so we expect the measured concentrations to be lower than the actual concentration. However this effect is likely negligible, and should continue the trend predicted on the graph.

To explore the relationship between CAP amplitude and $[K^+]_o$, the effects from simultaneous recordings in the same experiment are plotted on a semi-log graph in Figure 17C. This figure indicates an interesting correlation between the magnitude of potassium undershoot (i.e. concentrations lower than the physiological baseline of 3 mM) and the CAP amplitude. Low potassium concentrations seem to cause the increase in CAP amplitude. Observing the orange ($[K^+]_o$) and blue (CAP) data points, one can notice the similar trends between the frequencies, so although the standard deviations are large, the mean line of best fit provides a good indication of the overall positive correlation. Whereas the falling phase in CAP and biphasic profile of the $[K^+]_o$ response during stimulation are not similar enough to indicate potassium is the cause of this phase; the recovery responses follow similar profiles and appear to affect one another. Therefore, the role of potassium in the recovery phase of the action potential (and CAP) should be further investigated.

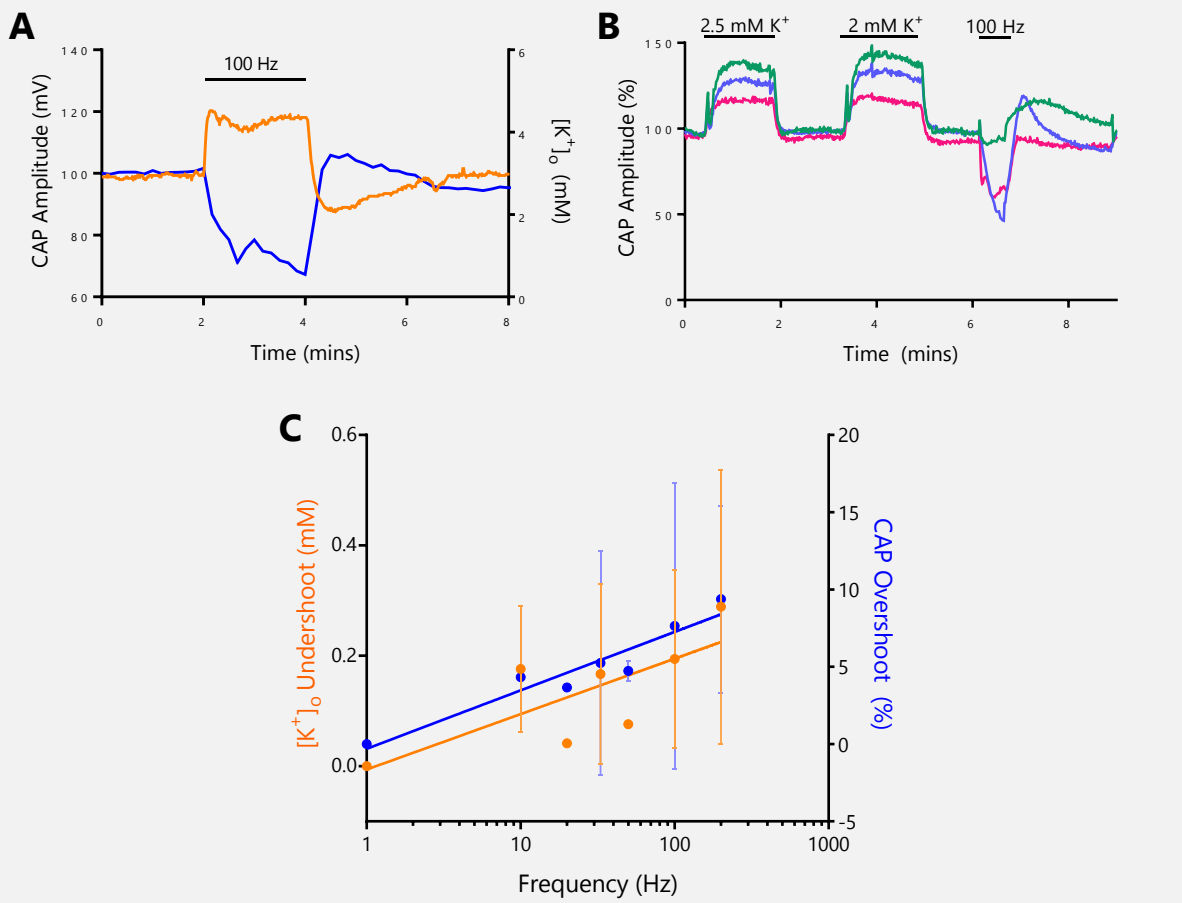

Figure 17. Correlation between the CAP overshoot, and extracellular potassium concentration ($[K^+]_o$) undershoot in recovery from high frequency firing, **A**. Technically difficult simultaneous recording of the CAP peak 2 response (blue) and the $[K^+]_o$ (orange) to a 2 minute stimulation at 100 Hz. The profile of the responses, although inversely related, follow unique patterns, indicating they are not causationally related. $[K^+]_o$ shows a biphasic response and an undershoot, whilst the CAP amplitude exhibits a singular falling phase followed by a recovery phase and overshoot. Ignore the artifact at ~ 2.5 mins (n = 1). **B**. Tri-peak CAP amplitude response indicating a correlation between low extracellular potassium concentrations ($[K^+]_o$) and the CAP overshoot following stimulation. $[K^+]_o$ was decreased from 3 to 2.5 and 2 mM, and the nerve stimulated at 100 Hz for 5 minutes (green = peak 1, blue = peak 2, red = peak 3; n = 1). **C**. Correlation between low extracellular potassium ($[K^+]_o$, high undershoot), and an increase in magnitude of the CAP overshoot. Plotting frequency on a logarithmic scale shows a positive relationship between $[K^+]_o$ undershoot and CAP overshoot with frequency. Note that the data was collected from the same nerves simultaneously, hence the similar variation pattern between data points. The potassium data is the same as Figure 15bii transformed to a magnitude of change from baseline, rather than actual concentrations, with 67 Hz omitted (mean ± SD, N = 7).

4 Discussion

In this thesis, we show that large axons are more resilient to metabolic challenge, sustaining firing at higher frequencies compared to smaller axons. We use *ex vivo* electrophysiological experimental data of MON preparations to show that the sub-population of small axon size (Peak 3) is susceptible to CAP amplitude drop using a metabolic challenge of just 10 Hz frequency stimulation. Applying both direct and indirect methods we suggest that, rather than elevated extracellular potassium, it is increased $[Na^+]_i$ that underpins the reduction in peak amplitude and change to the action potential profile, as predicted by the Nernst equation. Coincidentally, this conclusion was similarly reached in a modelling paper by Marder and Zang (2021), suggesting that large axons can support higher frequency firing.

4.1 Changes to the ionic concentrations underpin drop in CAP peaks

We show that the metabolic challenge causes the CAP peak amplitude to reduce in a frequency-dependent manner (Figure 14B). Neuronal firing relies upon the maintenance of specific intracellular ionic concentrations. The Nernst equation describes the movement of ions based upon the ionic concentrations, therefore experimentally changing the extracellular ion content provides a test for the responses of specific ions, in our case sodium and potassium. For the purposes of ease of understanding and basic principles, the Nernst equation will be used as the model in reference to the movement of ions. Many authors have accepted this as standard for the type of research, and despite the objections from others who claim the Goldman–Hodgkin–Katz equation should be used, there does not appear to be sufficient reason at this stage of exploratory research for more complex equations to be used.

We show the CAP profiles are affected by reduced $[Na^+]_o$ (Figure 15A) and increased $[K^+]_o$ (Figure 16C) experiments, where we control the extracellular concentrations of ions to alter the ionic gradients and thus the action potential profiles. Changing the ion concentrations alters the reversal potential for the contributing ions e.g. sodium (explored in Figure 15C), which distorts the shape of the action potential. This principle is supported by the work by Hodgkin and Katz (1949) who used the Nernst equation to predict the changes in the action potential amplitude, when $[Na^+]_o$ was reduced in the bathing sea water. This was determined by values for E_{Na}, mirroring their experimental findings of the peak amplitude response to reduced $[Na^+]_o$. The peak amplitude gets smaller consistent with the Nernst equation, and the rate of rise of the action potential gradient decreases which is directly proportional to $[Na^+]_o$ (Hodgkin & Katz, 1949). The early findings from this experiment substantiate the sodium theory of the action potential, guiding the work of Hodgkin and Huxley into the exploration of the underlying currents in the squid giant axon. The application of similar protocols to those described on MON, gives an insight into the responses of the mammalian systems and biological responses to metabolic challenge. We show that the MON CAP diminishes in a logarithmic manner relative to $[Na^+]_o$ (Figure 15C), as predicted by the Nernst equation, causing the peak to get smaller. We also show a differential sensitivity of the axon subpopulations to high frequency firing, with the small axons (peak 3) most susceptible, and large axons (peak 1) most resilient, to the metabolic challenge. Figure 18 shows the overlay of CAP profile to high frequency firing, aCSF low $[Na^+]_o$, and aCSF high $[K^+]_o$. Note that the profile of peak 3 is most similar between high frequency (blue) and low $[Na^+]_o$ (pink), indicating a

common mechanism that affects the peak amplitude and rate of rise. The similar trace responses support a common mechanism. This introduces an important consideration for the functional role of axon diameters: are large axons present to increase conduction velocity, or could they provide a metabolic support for intense firing.

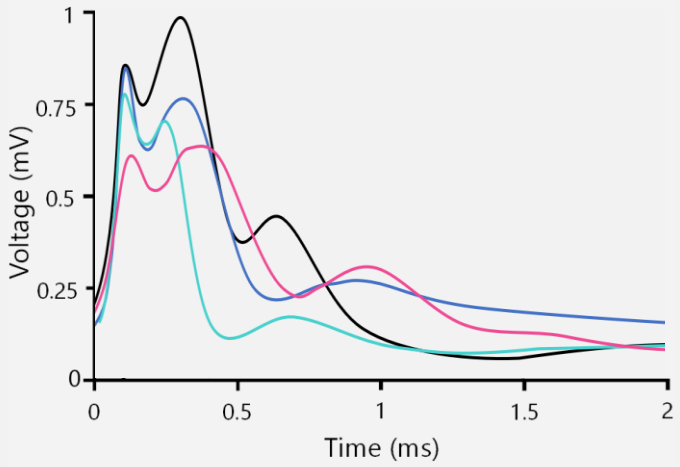

Figure 18. Overlay of example CAP profiles to show the effect of experimental protocols on the same nerve preparation: baseline CAP in normal aCSF 1 Hz (black), high frequency firing (40 Hz, blue), low sodium aCSF concentration (40 mM, pink), high potassium aCSF concentration (9 mM, turquoise) (n = 1).

The MON model for central white matter neuronal firing necessitates CAP recordings, rather than individual axon responses due to its small size. A three-month optimisation of the CAP set-up enabled stable recordings of the MON tri-peak profile, to study the response of the peaks in more detail than has been conducted previously. Other studies observing the effects of metabolic insults on the MON have explored the response to total 'CAP area' without determining which axons are affected (Brown *et al.*, 2003). We recorded the response of the CAP peak amplitudes to high frequency firing. We know from previous use of the MON under metabolic challenge, that the reduction in CAP amplitude is due to changes in the profile of action potentials produced by individual axons, as opposed to a loss of firing capacity of axons. If the firing capacity of individual axons was lost during high frequency firing, the peak amplitudes of the CAP profile would be reduced, without exhibiting 'slumping' in Figure 14D (particularly peak 3). Given an intense enough metabolic challenge (i.e. 100 Hz), all three peaks in the CAP exhibit slumping. This indicates that the mechanism causing the change in profile is occurring due to Nernstian changes in the relative ion concentrations across the axon membranes: due to alterations in the profile of individual action potentials. Furthermore, the differential response of peaks, with small axons affected first, predicts that it is the intracellular concentrations of ions that underpins the CAP drop.

4.1.1 Effect of $[K^+]_o$ on CAP profile

Hodgkin and Frankenhaeuser concluded that increased $[K^+]_o$ caused the squid giant axon action potential to drop. In Figure 16Bi, we show that during CAP amplitude reduction under intense firing at high frequencies, MON $[K^+]_o$ rises by a maximum of ~1 mM, from the baseline

of 3 mM. This is a small increase given the capacity for the $[K^+]_o$ to increase significantly since the $[K^+]_i$ is present at 100 mM, and during every action potential potassium leaves the cell. Bay and Butt (2012) found that MON $[K^+]_o$ increases by 1.6 mM following stimulation, whereas Ransom *et al.* (2000) found that $[K^+]_o$ increases by 3 mM following stimulation. This disparity is likely due to the model system used. This thesis used the same model as Bay and Butt (MON) and recorded similar concentrations; whereas Ransom *et al.* used the rat ON which is significantly larger in size.

Large increases in $[K^+]_o$ lead to membrane depolarisation, which among other effects, causes inactivation of sodium channels. Sodium channels have an innate inactivation mechanism that prevents hyperexcitability and excessive firing, and facilitating homeostatic equilibration of the ionic gradients (Hodgkin & Huxley, 1952; Somjen, 1979). Hodgkin and Huxley calculated the inactivation curve for sodium using a double-pulse protocol; plotting the conditioning pulse potential against the steady state sodium currents produces a sigmoidal curve, with the resting membrane potential correlating to ~40% inactivation (Hodgkin & Huxley, 1952; Brohawn *et al.*, 2019). This means that a small shift in the membrane potential above or below the resting potential significantly affect the number of inactivated sodium channels, since the membrane potential falls in the middle of the steep inactivation curve (see Figure 19). The time course for sodium channels to recover from inactivation, from -85 mV resting potential at 37°C, is 4 - 5 ms (Schwarz, 2021). This interval supports firing of up to 200 Hz, which we showed only caused a 20% drop in CAP amplitude for peaks 1 and 2, but a 40% reduction for peak 3 (Figure 11A). An example of how changes to channel conductance can affect the CAP peak amplitude under rest conditions was explored by Kanda *et al.*, in regards to K2P channels. These channels control the movement of potassium ions across the membrane, so when K2P conductance was lowered, the interval required for following action potentials to present full profiles increased, with CAP peak amplitude reduction occurring at significantly lower frequencies (Kanda *et al.*, 2019).

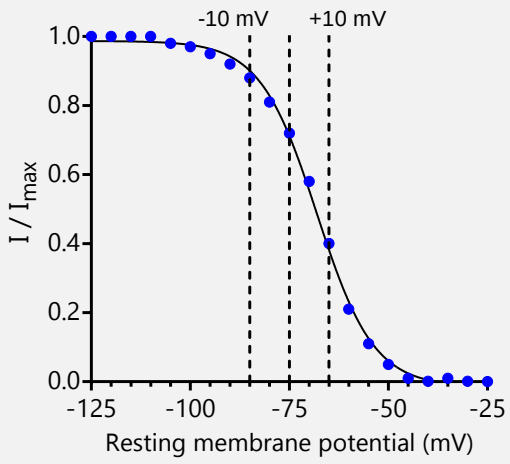

Figure 19. Steady-state Na_V inactivation curve plotted against membrane potential. Dashed lines indicate 10 mV deviations from the resting potential, showing how small changes in voltage produce a large effect on channel inactivation. Data reproduced from Figure 7C and D (Brohawn *et al.,* 2019).

In Figure 16D we show that the CAP profile reduces in total amplitude across all three peaks, and the rate of rise similarly reduce, with $[K^+]_o$ from 9 mM and greater. High $[K^+]_o$ reduces Na_V channel availability for future firing, so the sodium ions have fewer channels to move through, resulting in a slower rate of depolarisation in the action potential and a smaller peak amplitude. This could explain the reduction in CAP. During high frequency firing, however, the magnitude of $[K^+]_o$ reached in any of the experimental recordings did not increase above 4.5 mM.

Following stimulation, the $[K^+]_o$ profile undershoots, with the concentration dropping below baseline (Figure 16A). Reductions in $[K^+]_o$ below 3 mM causes membrane hyperpolarisation, which relieves the inactivation on sodium channels. This means that more channels are available to be recruited in the action potential, so more sodium ions can cross the membrane in the direction that takes the membrane potential towards the E_{Na} (influx) due to the increased number of open channels. The result of this is that the rate of depolarisation is much faster and the peak amplitude increases (Figure 17B: 2.5 and 2 mM $[K^+]_o$). In other words, reduction in $[K^+]_o$ causes E_K to become more negative: $E_K = 61.5 \log (\downarrow[K^+]_o/[K^+]_i)$. $[K^+]_o$ is initially lower than $[K^+]_i$, so when the logarithmic relationship is accounted for, going from 3 mM to 2.5 mM $[K^+]_o$ after a period of intense stimulation in MON, would cause E_K to go from -94 mV to -99 mV. Despite this being only a 5 mV change, the same relative increase (0.5 mM) in the $[K^+]_i$ to 100.5 mM, results in a 0.1 mV hyperpolarisation. This emphasizes the influence of small $[K^+]_o$ reductions on the membrane potential (and thus inactivation of sodium channels), due to the Nernstian and logarithmic relationship between the ratio of intra and extracellular ionic concentrations. Figure 17C shows the post-stimulus response of $[K^+]_o$, using simultaneous measurements, and shows a correlation between the reduction in $[K^+]_o$ and increase in CAP amplitude. The mechanism described above could explain how this occurs, when changes to the extracellular concentrations alter the response and activity of axons irrespective of diameter. See the summary in Figure 20 which alludes to post-stimulation recovery, where all three peaks reach the same CAP overshoot, irrespective of how much the amplitude dropped during firing (data not shown). This indicates that reductions in $[K^+]_o$ can affect all peaks to the same extent, which does not explain the differential sensitivity of axon populations to high frequency firing.

4.1.2 Proposed effect of $[Na^+]_o$ on the differential drop in cap peak amplitudes

Large axons have a high membrane area to axoplasmic volume ratio, supporting the influx of a larger number of ions before the concentration is altered to any significant degree. The increased membrane area raises the number of Na/K pumps which ease ion re-equilibration, and prevents the sodium influx accumulating as quickly, keeping the $[Na^+]_i$ lower for longer. Figure 15D shows how the same stimulus intensity can have a significantly different effect on the corresponding predicted $[Na^+]_i$ between large and small axons.

Increases in $[Na^+]_i$ cause E_{Na} to decrease given that the $[Na^+]_o$ is maintained at 155 mM in the aCSF bathing the nerve. E_{Na} is determined by the concentrations of sodium either side of the membrane, so increasing $[Na^+]_i$ causes a predictable reduction in E_{Na} to a value referred to as $E'_{Na.}$ As concluded by Hodgkin and Katz (1949), the peak of the action potential is driven by E_{Na}, so when E'_{Na} is reduced, the peak amplitude decreases. During a train of action potentials, if the stimuli are sufficiently far apart, the Na/K pump can adequately re-equilibrate the ion

gradients and maintain the peak amplitude. However, if the firing interval is too short, the Na/K pump is unable to maintain the gradients and sodium ions accumulate in the axon, increasing $[Na^+]_i$, and shifting E'_{Na} less positive as the peak continues to fall. Another consequence of increasing $[Na^+]_i$, is the driving force of sodium ions to enter the axon decreases as the concentration gradient is lower. This causes ions to flow at a slower rate into the axon, despite the normal channels opening, and therefore causes the rate of rise to decrease and the action potential profile to spread out.

Axonal $[Na^+]_i$ is dependent upon sodium influx during the action potential, and the efflux via the Na/K pump. If the Na/K pump copes with the rate of efflux required to maintain $[Na^+]_i$ around 10 mM then the CAP shouldn't fail. Observations that the third peak fails before the second and first indicates that the efflux mechanism is not sufficient to maintain the concentrations at 30 Hz firing frequency etc. Rate constants are used in physiology to describe the time frame of biological processes, such as the activity of ion channels or pumps. Specifically, the rate constant describes the point at which 37% of the maximum rate occurs, therefore two processes with relatively similar rate constants indicates a similar underlying mechanism. In the realm of this experiment, one could propose that the rate of sodium ion accumulation in the intracellular space is similar to the drop in the CAP, the reduction in peak amplitude during trains of action potentials could be related to the capacity of the Na/K pump. Future research could explore the falling and recovery phases of the CAP peak amplitudes over time, to determine if the rate constant changes.

If the CAP amplitude falls due to increased $[Na^+]_i$, could the post-stimulation CAP overshoot occur due to a decrease in $[Na^+]_i$? Lowering the $[Na^+]_i$ from 30 mM to 20 mM, would cause the E_{Na} to increase from +44 mV to +55 mV, that would facilitate a larger action potential magnitude. However, it is evolutionarily unstable for this to occur, due to the mechanisms at play: a clearance mechanism pumping out sodium would not work at a faster rate than the influx mechanism. Particularly if the clearance mechanism (the Na/K pump) rate is affected by $[Na^+]_i$, whereby when the concentration approaches the resting $[Na^+]_i$ of ~10 mM, the rate slows to coincide with the homeostatic regulation of the resting membrane potential. In regards to the osmotic role of sodium, a reduction in the intracellular concentration below the baseline would affect the cell, disrupting normal functional ability of the axon and would likely affect the ability of axons to fire action potentials.

The conclusions made in this thesis are graphically represented in Figure 20 showing the nerve response to 100 Hz stimulation for 5 minutes. From the top, we show the measured $[K^+]_o$ (turquoise), CAP peak amplitudes (red: peak 1, blue: peak 2, green: peak 3), and individual CAP profiles (black), and the calculated $[Na^+]_i$ (pink) indicated across the three peaks and axon subpopulations. We conclude that the reduction in CAP amplitude is a result of increasing $[Na^+]_i$, with small axons susceptible to sodium accumulation at lower frequencies, due to the Na/K pumps present on the membrane unable to maintain the ionic concentration gradients.

We strongly indicate that the CAP overshoot post-stimulation is likely due decreases in $[K^+]_o$.

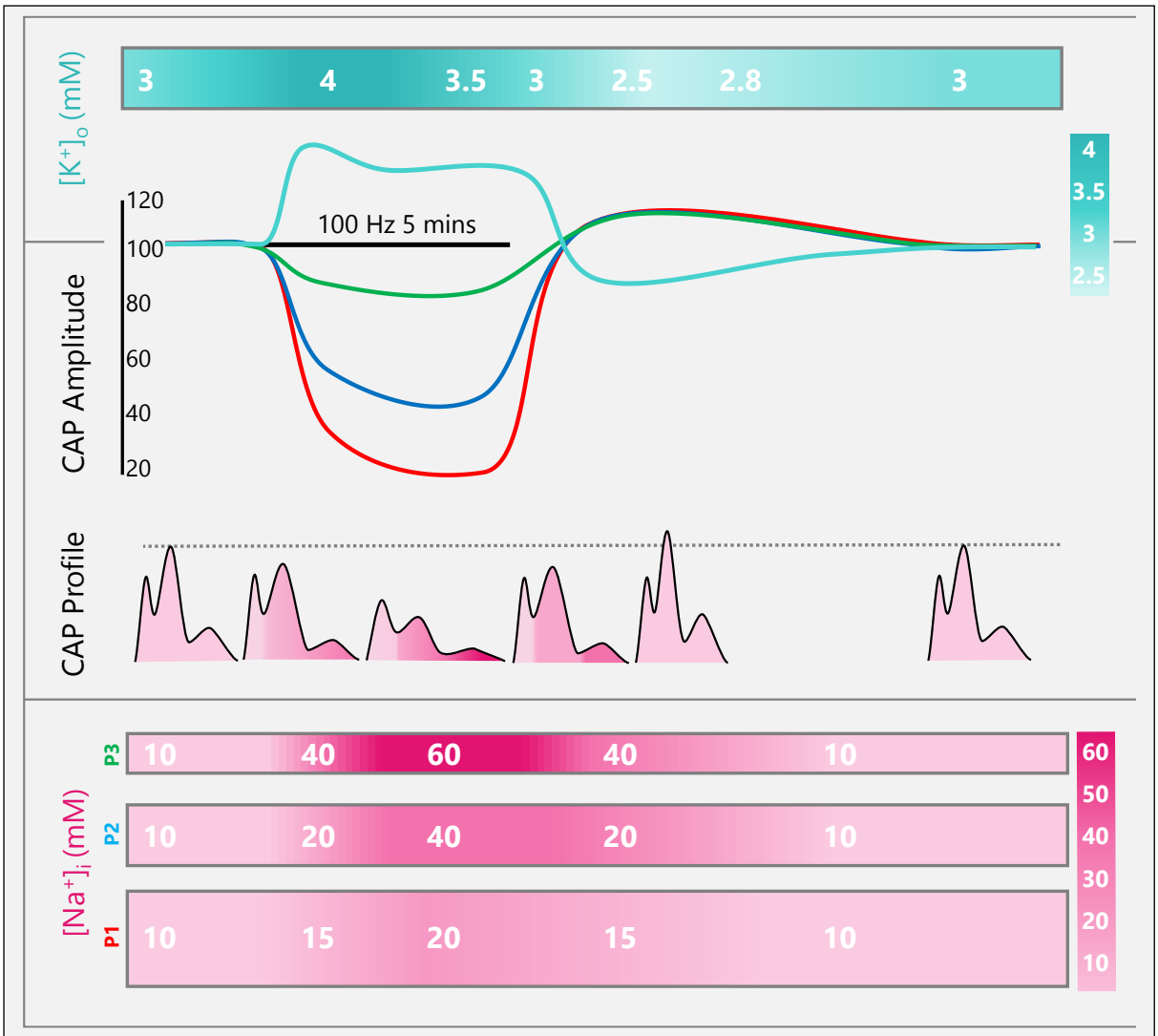

Figure 20. Summarised typical nerve response to 100 Hz stimulation for 5 minutes. Extracellular potassium concentrations ($[K^+]_o$) and the profile of the response (turquoise) are exhibited, showing the typical biphasic peak and undershoot. The compound action potential (CAP) amplitudes illustrate the differential drops in CAP amplitude (black scale) for peak 1 (green), peak 2 (blue), and peak 3 (red). Illustrative CAP profiles are shown in response to high frequency, highlighting the overshoot during recovery. The CAP profiles are coloured with the intracellular sodium concentrations ($[Na^+]_i$), of the peaks, mirrored in the three traces of increasing diameter that are plotted alongside the concentration scale.

4.2 Functional benefits of axon diameter

We found a correlation between frequency and reduction of the action potential peak due to axon diameter; in support of this relationship, Zang and Marder (2021) predicted the effect of high frequency firing on unmyelinated and myelinated axons and concluded that large axons could be more resilient to this metabolic challenge. Zang and Marder (ZM) modelled the effect of three frequencies (1, 30, and 60 Hz) on the change in $[Na^+]_i$ and E_{Na} for three myelinated axon diameters 0.2, 0.6, and 1.0 µm, which is comparable to our calculations for the three axon subpopulations peak 3, peak 2, and peak 1 respectively. Table 1 compares the predicted values

from this study to the experimental recordings collected in the present thesis. The strong similarity of the experimentally recorded data to the other authors' model provides strong support for the findings concluded here, particularly the differential sensitivity of the axons to the metabolic insult occurring due to the axon diameters. Since this model is exploring the general effect on 'axons', the resemblance of data to this thesis helps validate the MON as a model for central white matter axons throughout the mammalian system. This highlights the useful application of rodent nerve models to understanding the normal physiology of electrical cell signalling. ZM modelled the beneficial effect of myelin on ionic diffusion and responses of ion equilibration at the nodes, determining that nodes facilitate equilibration at a faster rate than in unmyelinated axons. The unmyelinated axons failed to conduct action potentials for any long duration, with $[Na^+]_i$ exponentially increasing and causing failure of firing. When the factor of sodium ion diffusion into the paranodal regions was introduced, the myelinated model supports firing of action potentials up to high frequencies. This supports the metabolic role of myelin, whereby equilibration only has to occur at the nodes, with the internodal regions providing axoplasmic space for ionic diffusion. ZM reach the same conclusion we do here, that alterations in CAP are a result of $[Na^+]_i$: as stimulation rate increases, the magnitude of $[Na^+]_i$ increases more quickly in small axons, and faster with frequency.

Table 1. Comparison of conclusions predicted by ZM ((Zang & Marder, 2021) Figure 3E) to the experimental data collected in the present thesis, of the intracellular sodium concentration ($[Na^+]_i$) and reversal potential (E_{Na}) in response to firing frequency in different axon diameters. Large axons are classed as 1.0 µm or peak 1, intermediate as 0.6 µm or peak 2, and small as 0.2 µm or peak 3.

Frequency (Hz)	**Axon size**	**$[Na^+]_i$ (mM)**		**E_{Na} (mV)**	
		ZM	Present thesis	ZM	Present thesis
1	Large	18	10	60	70
	Intermediate	18	10	58	70
	Small	18	10	58	70
30	Large	20	14	58	64
	Intermediate	25	17	50	59
	Small	42	41	35	35
60	Large	22	17	58	58
	Intermediate	27	26	48	46
	Small	~50	59	~30	25

We converted our experimental data into the relative $[Na^+]_i$ and E_{Na} (Figure 15C). At rest, 1 Hz, we assume the $[Na^+]_i$ is 10 mM (Ransom *et al.*, 2000), and the resting E_{Na} is 70 mV. At 30 Hz, we show that the $[Na^+]_i$ accumulates to different amounts depending upon the relative axon diameter: in small axons it reaches 41 mM (ZM modelled 42 mM), in intermediate axons it reaches 17 mM (ZM modelled 25 mM), whereas in large axons it only increases to 14 mM (ZM modelled 20 mM). The sodium concentration in large axons only increases by 4 mM from the baseline, which is a small concentration change therefore in agreement with the $[Na^+]_i$ theory,

it follows that peak 1 shows minimal CAP reduction at 30 Hz (Figure 14B). Likewise, at 60 Hz, the peaks respond in a differential manner coinciding with the trend predicted by ZM, with the small axon $[Na^+]_i$ increasing to 59 mM (ZM modelled ~50 mM), the intermediate to 26 mM (ZM modelled 27 mM), and the large axons showing only a small increase from the response to 30 Hz.

It is important to acknowledge some of the differences between the model and data collection in this thesis. First, for $[Na^+]_i$ magnitude responses calculated for stimulations at the specified frequencies, the 'spike' numbers were used to determine the duration of responses, using 5000 as the maximal response and highest metabolic insult. In this thesis, we altered the stimulus frequency whilst maintaining the same duration, which means that our results include increasing spike numbers alongside frequency. 5000 spikes is equivalent to 83 seconds stimulation at 60 Hz and 160 seconds at 30 Hz. The average durations used to calculate $[Na^+]_i$ data was between 120 and 240 seconds, therefore this factor appears to be a different method for testing metabolic challenge rather than a weakness or oversight in the methodology. The most noticeable deviation in the results collected from the predictions occurs from peak 1 (large axons) which is understandable given the relatively small magnitude of $[Na^+]_i$ increase. Second, our use of a supramaximal stimulus directed from the stimulating suction electrode along the nerve to the recording electrode ensures that action potentials in all axons are stimulated initially. Can we be sure that all of these action potentials successfully propagate down the entire nerve? ZM highlight this issue, modelling that in the smallest axons of 0.2µm at 60 Hz, 50% of the action potentials successfully propagate down the myelinated nerve, and at 90 Hz only 25% propagation occurs (see ZM Figure 3D 1 and 2).
Third, another factor that proves inconsistent between our conclusions is the axonal response at 1 Hz. ZM modelled that irrespective of diameter, all axonal $[Na^+]_i$ would increase to 18 mM following 5000 spikes (equivalent to 83 minutes stimulus duration). We followed the assumption by Bay and Butt (2012) and Ransom *et al.* (2000) that 1 Hz is a low enough frequency to pose no metabolic challenge and prevent any form of $[Na^+]_i$ accumulation, hence we assume it is 10 mM. This is supported by experiments using a minimum stimulation of 1 Hz for 160 minutes and observed no drop in the CAP, e.g. see Figure 14C low and high frequency where the experiments were conducted consecutively on the same nerve. We found that the same nerve could be used for up to 8 hours, with no noticeable tiring of the CAP in response to conditions of metabolic firing, retaining the baseline profile (data not shown). Applying our experimental findings indicates that the predictions by ZM may have underestimated the capacity for axons to recover, and we support the assumption that $[Na^+]_i$ does not increase at 1 Hz.

In 2009, Perge *et al.* investigated the differences in function based on axon diameter of the optic nerve, and concluded that large axons are required to facilitate fast rates of information transduction at the synapses through having large terminal arbors and active zones. This further indicates that large diameter axons in the optic nerve are not likely present to support a faster conduction velocity, and instead support a higher metabolic capacity. Within this same paper the conclusion was made that 'sodium buffering does not explain the need for larger axons' (Perge *et al.*, 2009). Using a previously published model made in NEURON by one of the authors, the change in $[Na^+]_i$ for 0.2 µm axons remained at 11 mM during 100 ms duration

when diffusion into the internodes was accounted for (Perge *et al.*, 2009). This conclusion may be correct for the application of such a small train of stimulus, at 300 Hz for 0.01 of a second. However, particularly when acknowledging the optic nerve model used, the cells will be active a large percentage of the time, therefore modelling the responses of the cells after durations longer than fractions of a second is pertinent. More recently, Zang and Marder (2021) did indeed model responses of firing in different time frames from 1.38 to 83 minutes, to computationally explore the effect of myelination, firing rate, and spiking.

In the optic nerve, specific cell types could have functional roles which have been driven by axon diameter. Three cell-types in the optic nerve were modelled to compare the cost of transmitting a set amount of data (300 bits per second), across bundles of axons of the same type (Koch *et al.*, 2006). It was modelled that a bundle of 35 'local-edge' cells firing at 4 Hz would only require ~140 spikes per second each to transmit this information, able to confer 2.1 bits per spike. Whereas the theoretical 'high rate channel' cells (~7 axons) firing at 40 Hz would require ~270 spikes per second per cell, with each spike only contributing 1.1 bit per spike (Koch *et al.*, 2006). The increased spike rate correlates to a higher metabolic cost (Attwell & Laughlin, 2001), so cells that confer information at a higher rate would need to have mechanisms that support this metabolic demand, i.e. larger axon sizes. This model supports our conclusion: that the large axons are more resilient to high frequency firing, and could have been evolutionarily maintained by having a higher metabolic resilience as opposed to a faster conduction velocity. Acknowledging the number of axons required for these processes and firing rates at different frequencies supports the morphological trends observed in the axon distributions. Transferring 300 bits per second at 4 Hz would require 35 cells/axons, whereas transferring this information at 40 Hz would only require ~7 cells/axons (Koch *et al.*, 2006). The increased prevalence of small axons is supported by the calculations made by previous authors, historical data, and confirmed in this research in Figure 11B, with a distribution of axon diameter skewed towards smaller axon sizes.

4.3 MON as a model for central white matter

Previously published electron microscopy cross section images of central white matter (rodent optic nerve) highlight three key factors (Allen *et al.*, 2006). The first being that the proportion of small axons in the optic nerve is significantly more than the proportion of large axons. Figure 11B shows the distribution skewed towards small axons, with the mode occurring at 0.7 µm. The second is that the extracellular space is very small; axons are practically pressed against one another, despite the varying diameters, resulting in a small interstitial space. The third is the absence of axonal clumping, which is observed in the sciatic nerve. There are several extra layers of membrane: the endoneurium wraps the sciatic axons and Schwann cells, and the perineurium encases bundles of these cells, e.g. forming small c-fibres fascicles (Pavelka & Roth, 2010). These morphological characteristics lead to functional effects that implicate the present study.

The small extracellular space is particularly important in regards to the role of $[K^+]_o$ on functional capacity of axonal firing. In the squid giant axon, the presence of the extra membrane produced a small volume of space outside the axon, that facilitated the accumulation of potassium ions and therefore affected the amplitude and maintenance of

future action potentials (Frankenhaeuser & Hodgkin, 1956). In the MON, the small extracellular space between axons means that the high firing rate of one neuron could affect the neighbouring cells due to shared extracellular space. The presence of glia has a huge role in minimising the increases in $[K^+]_o$ with substantial spatial buffering occurring throughout the syncytium. In the squid, the lack of myelin results in action potentials which have to propagate along the entire axon in a wavelike progression, causing a widespread change in ionic concentrations in the extracellular space (Frankenhaeuser & Hodgkin, 1956). All MON axons are myelinated, so the propagation pattern is different, needing to only occur at the nodes. Therefore when firing, the main increases in $[K^+]_o$ occur at the nodes, coincidentally (or not) the precise location of the astrocyte processes.

Consider the effect of axon diameter on myelination. All node lengths are the same, but the internode distances vary dependent upon diameter (Arancibia-Cárcamo *et al.*, 2017). This means that small axons have proportionally more nodes than larger axons, therefore when running parallel the nodes of axons of varying diameters will not align. Therefore, the localised responses of one axon to the extracellular space will not necessarily affect the axon neighbours if there is a layer of myelin in close vicinity. Interestingly, we show that during high stimulus intensity, the $[K^+]_o$ increases by ~1 mM, and following recovery and removal of the stimulus, the $[K^+]_o$ undershoots the baseline by ~0.5 mM (Figure 16Bi,ii). The reduction in $[K^+]_o$ is attributed to the activity of glial Na/K pumps, working to pump potassium into the astrocytes, removing it from the extracellular space. The correlation between reduced $[K^+]_o$ and the CAP overshoot (Figure 17C) across all three peaks indicates that following a sufficiently long duration, the $[K^+]_o$ affects all the axons leading to the increase in CAP amplitude, irrespective of diameter. This supports our conclusion that high frequency firing affects the $[K^+]_o$ at the nodes, which has minimal effects on the activity of other axons, however with long durations this effect can be spread throughout the nerve irrespective of diameter. In situations of metabolic challenge, the action potentials of individual axons is affected due to increased $[Na^+]_i$, and following long enough stimulation, the reduction in $[K^+]_o$ in the extracellular space can affect neighbouring cells too.

There is a historical precedent to use the MON as a central white matter model, with investigation providing a wealth of knowledge about this mammalian nerve, to aid understanding of human white matter physiology. The high frequency firing model for metabolic challenge in MON provides useful physiological data. Although some of the durations and frequencies of firing are unphysiologically high, we can assume that the mechanisms in place that facilitate the firing and recovery (particularly note the $[K^+]_o$ undershoot and CAP overshoot) are innate and present within all myelinated central axons. The mice used in the study are CD1, and were selected as a strain with no obvious/clear genetic malfunctions/disruptions, therefore provide a representative model of central white matter. Interestingly, C57 mice were used for one week, and the CAP profile shows a change, with the first peak larger than the second peak i.e. contains a larger number of large axons compared to the model used in this thesis (data not shown). Future studies could explore the differences in CAP profiles and aim to explore how the axon diameters of the MON are strain dependent. C57 is used in stroke research and thus could have defects in the visual system. In regards to general MON *ex vivo* preparation, care must be taken to prevent the nerves being stretched

which could alter normal physiological function and channel activity. K2P channels are affected by mechanical stretch, with increased tension on the membrane causing increased currents through the channels to compensate for ectopic action potentials produced by stretch, and hyperpolarising the membrane to accommodate (Brohawn *et al.*, 2019).

It is assumed that the highest CAP amplitudes would occur at the lowest firing rate (1 Hz), since this provides more than adequate time for ion equilibration and the resting membrane potential to be reinstated. Observe the CAP amplitude responses to 5 Hz in Figure 14B, and the response of peak 1 in Figure 14C, to note that the CAP increases in amplitude from baseline stimulation at a frequency of 5 Hz. This phenomenon occurred in multiple nerve experiments, which indicates that there could be a physiological basis for this response, as opposed to an experimental artifact. One could posit that some axons in the nerve might have an optimal firing rate at 5 Hz, rather than 1 Hz which is logically assumed to be the optima. Koch *et al.* (2006) propose that the cell types in MON are designed to function optimally at different frequencies, supporting this theory of a differential activity baseline dependent on diameter (Koch *et al.*, 2006). This indicates that axonal capacity for peak CAP amplitude firing may lie on a bell curve, with an evolutionarily determined optimum firing rate that differs in axons to support firing. Future experiments should examine the low frequencies in more detail to determine if the CAP peak amplitudes do in fact decrease at frequencies lower than 1 Hz, though at this stage these investigations may not unveil any important characteristics.

The study by Dutta *et al.*, (2018) indicate a direct role of perinodal astrocytes altering the myelin and nodal lengths on individual axons, due to exocytosis of factors (thrombin-mediated cleavage of NF155) in the node. Using electrophysiological techniques, the release of these factors was shown to decrease the conduction velocity of action potentials in MON (Dutta *et al.*, 2018). They suggest that this is important when considering neural oscillations in distant regions of the brain, where conduction delays must be accounted for to maintain firing patterns, and astrocytes could innately modulate this process (Khodagholy *et al.*, 2017). This study did not explore how astrocyte remodelling could be affected by neuronal activity. Genetic knockouts of factors associated with the perinodal astrocytes were found to cause no changes to the axon diameters or number of axons within the MON, indicating this could have a pre-determined biological metabolic functional role, and isn't set to be purely determined by conduction velocity. Relating the responses of axons in the MON model, to the function of these cells *in vivo*, is a consideration that should be further explored to better understand how the evolution of structural factors (axon diameter) aids function of generalised cell signalling in the central nervous system.

The model of metabolic challenge used in this study was high frequency firing. Previous authors have used alternative methods such as changing the metabolic substrates in the aCSF to exacerbate energy stores in the nerves to study how the total CAP area is affected. Brown *et al.* (2003) tested the resilience of MON to zero glucose, using 1 Hz frequency stimulation, and found that the CAP area dropped after a delay that lasted longer than the time taken for the zero glucose solution to wash over the nerve. This occurred due to the neuro-glial interactions, with glycogen stores present in glial cells able to support normal firing in the absence of glucose for a short duration (Brown *et al.*, 2003). This thesis shows a differential

sensitivity of the tri-peak profile to metabolic challenge, so it would be interesting to reproduce substrate-experiments to determine if the axon diameter affects the response to this form of insult. It could be predicted that the CAP amplitude reduction would affect the peaks differently. The astrocytic release of lactate (from glycogen stores) helps provide a substrate replacement for glucose during intense activity (Brown *et al.*, 2003, 2012), however the lactate may be preferentially taken up by one sub-population of axons, e.g. small diameter axons to support firing given that the proportion of mitochondria is smaller given the relatively small axoplasmic volume.

Meakin *et al.* (2007) found that the first peak in MON is lost upon replacement of glucose with fructose (20 mmol/L), likely due to the lack of fructokinase enzymes that enable efficient metabolism of this substrate. The second and third peaks are unchanged by this replacement and maintain optimal firing capacity (Allen *et al.*, 2006; Meakin *et al.*, 2007). This provides both an interesting consideration for the differences in metabolic capacity of the axons, and could provide a new method to accurately explore the effect of high frequency firing on the first peak, were the conditions repeated in glucose and fructose environments, with the second and third peak responses subtracted from the total CAP. In the present study, fitting the CAP with Gaussian distributions appears valid and sufficient to combat the overlap between the first and second peaks (Figure 10).

4.4 Conclusion

The action potential relies on ionic gradients to be rigidly maintained and transiently altered over time to allow the signal to carry over long distances without decaying. This research indicates that under high levels of nervous system activity, metabolic stress, and continuous trains of action potentials, the action potential profile can change. We show a differential response of axons to high frequency firing in the MON. Large axons appear more resilient to high frequencies, sustaining CAP amplitudes for longer before falling, and vice versa. Using indirect methods and potassium microelectrodes, we conclude that the cause of mammalian CAP peak amplitudes reducing is due to increases in $[Na^+]_i$, rather than increased $[K^+]_o$. Applying the technically difficult experimental technique, of simultaneously recording the CAP and $[K^+]_o$ response to nerve stimulation, provides convincing evidence that there is a correlation between the $[K^+]_o$ undershoot and CAP overshoot during post-stimulus recovery. Future experiments should explore the benefits of varying axon diameters, and use alternative nerve models, such as the mouse sciatic nerve, to better explore the physiological basis for maintaining CAP amplitudes in central and peripheral systems.

5 References

Allen L, Anderson S, Wender R, Meakin P, Ransom BR, Ray DE & Brown AM (2006). Fructose Supports Energy Metabolism of Some, But Not All, Axons in Adult Mouse Optic Nerve. *J Neurophysiol* **95,** 1917–1925.

Arancibia-Cárcamo IL, Ford MC, Cossell L, Ishida K, Tohyama K & Attwell D (2017). Node of Ranvier length as a potential regulator of myelinated axon conduction speed. *Elife* 6:e23329.

Armstrong CM (2003). The Na/K pump, Cl ion, and osmotic stabilization of cells. *Proc Natl Acad Sci U S A* **100,** 6257–6262.

Attwell D & Laughlin SB (2001). An energy budget for signaling in the grey matter of the brain. *J Cereb Blood Flow Metab* **21,** 1133–1145.

Bakken TE & Stevens CF (2012). Visual system scaling in teleost fish. *J Comp Neurol* **520,** 142–153.

Bay V & Butt AM (2012). Relationship between glial potassium regulation and axon excitability: a role for glial Kir4.1 channels. *Glia* **60,** 651–660.

Brohawn SG, Wang W, Handler A, Campbell EB, Schwarz JR & MacKinnon R (2019). The mechanosensitive ion channel traak is localized to the mammalian node of ranvier. *eLife* **8**:e50403.

Brown AM, Evans RD, Black J & Ransom BR (2012). Schwann cell glycogen selectively supports myelinated axon function. *Ann Neurol* **72,** 406–418.

Brown AM, Tekkök SB & Ransom BR (2003). Glycogen regulation and functional role in mouse white matter. *Journal of Physiology* **549,** 501–512.

Bullock TH, Moore JK & Fields RD (1984). Evolution of myelin sheaths: both lamprey and hagfish lack myelin. *Neurosci Lett* **48,** 145–148.

Camm JP (1986). The Chromatophore Lobes and their Connections in Octopus. *PhD Thesis*.

Crotty P, Sangrey T & Levy WB (2006). Metabolic energy cost of action potential velocity. *J Neurophysiol* **96,** 1237–1246.

Danowski TS (1941). The transfer of potassium across the human blood cell membrane. *Journal of Biological Chemistry* **139,** 693–705.

Drenhaus U, von Guntern A & Rager G (1997). Classes of axons and their distribution in the optic nerve of the tree shrew (Tupaia belangeri). *Anat Rec* **249,** 103–116.

Dutta DJ, Woo DH, Lee PR, Pajevic S, Bukalo O, Huffman WC, Wake H, Basser PJ, SheikhBahaei S, Lazarevic V, Smith JC & Fields RD (2018). Regulation of myelin structure and conduction velocity by perinodal astrocytes. *Proc Natl Acad Sci U S A* **115,** 11832–11837.

Edgar JM, McCulloch MC, Montague P, Brown AM, Thilemann S, Pratola L, Gruenenfelder FI, Griffiths IR & Nave KA (2010). Demyelination and axonal preservation in a transgenic mouse model of Pelizaeus-Merzbacher disease. *EMBO Mol Med* **2,** 42–50.

Edgar JM, McCulloch MC, Thomson CE & Griffiths IR (2008). Distribution of mitochondria along small-diameter myelinated central nervous system axons. *J Neurosci Res* **86,** 2250–2257.

Erwin DH & Davidson EH (2002). The last common bilaterian ancestor. *Development* **129,** 3021–3032.

Fern R, Davis P, Waxman SG & Ransom BR (1998). Axon Conduction and Survival in CNS White Matter During Energy Deprivation: A Developmental Study. *Journal of Neurophysiology* **79**, 95-105.

Frankenhaeuser B & Hodgkin AL (1956). The after-effects of impulses in the giant nerve fibres of Loligo. *J Physiol* **131,** 341–376.

Giaume C, Koulakoff A, Roux L, Holcman D & Rouach N (2010). Astroglial networks: a step further in neuroglial and gliovascular interactions. *Nat Rev Neurosci* **11,** 87–99.

Gleich O & Wilson S (1993). The diameters of guinea pig auditory nerve fibres: distribution and correlation with spontaneous rate. *Hear Res* **71,** 69–79.

Haeckel E (1892). *The History of Creation or the Development of the Earth and its Inhabitants by the Action of Natural Causes*. D. Appleton & Co., New York.

Hanke FD & Kelber A (2020). The Eye of the Common Octopus (Octopus vulgaris). *Front Physiol* **10,** 1637.

Hille B (1989). Ionic channels: evolutionary origins and modern roles. *Quarterly Journal of Experimental Physiology* **74,** 785–804.

Hille B (2001). Ion channels of excitable membranes. In, 3rd edn., pp. 1–22. Sinauer Associates, Sunderland, Massachusetts.

Hodgkin AL & Huxley AF (1952). The dual effect of membrane potential on sodium conductance in the giant axon of Loligo. *J Physiol* **6,** 497–506.

Hodgkin AL & Katz B (1949). The effect of sodium ions on the electrical activity of giant axon of the squid. *J Physiol* **108,** 37–77.

Honjin R, Sakato S ichi & Yamashita T (1977). Electron microscopy of the mouse optic nerve: a quantitative study of the total optic nerve fibers. *Arch Histol Jpn* **40,** 321–332.

Hopper A, Beswick-Jones H & Brown AM (2022). The Nernst equation: Using physico-chemical laws to steer novel experimental design. *Adv Physiol Educ* **46,** 206–210.

James EL, Peacock VAH, Ebling FJP & Brown AM (2010). Morphological and electrophysiological characterization of the adult Siberian hamster optic nerve. *Anat Sci Int* **85,** 214–223.

Jegla T, Grigoriev N, Gallin WJ, Salkoff L & Spencer AN (1995). Multiple Shaker potassium channels in a primitive metazoan. *Journal of Neuroscience* **15,** 7989–7999.

Kanda H, Ling J, Tonomura S, Noguchi K, Matalon S & Gu JG (2019). TREK-1 and TRAAK Are Principal K + Channels at the Nodes of Ranvier for Rapid Action Potential Conduction on Mammalian Myelinated Afferent Nerves. *Neuron* **104,** 960-971.e7.

Khodagholy D, Gelinas JN & Buzsáki G (2017). Learning-enhanced coupling between ripple oscillations in association cortices and hippocampus. *Science* **358,** 369–372.

Koch K, Mclean J, Segev R, Freed MA, Ii MJB, Balasubramanian V & Sterling P (2006). Report How Much the Eye Tells the Brain. *Current Biology* **16,** 1428–1434.

Kuffler SW, Nicholls JG & Orkand RK (1966). Physiological properties of glial cells in the central nervous system of amphibia. *J Neurophysiol* **29,** 768–787.

Liebeskind BJ, Hillis DM & Zakon HH (2011). Evolution of sodium channels predates the origin of nervous systems in animals. *Proc Natl Acad Sci U S A* **108,** 9154–9159.

Macallum AB (1926). The Paleochemistry of the body fluids and tissues. *Physiology Reviews* **6,** 316–357.

Maingret F, Lauritzen I, Patel AJ, Heurteaux C, Reyes R, Lesage F, Lazdunski M & Honoré E (2000). TREK-1 is a heat-activated background K+ channel. *EMBO J* **19,** 2483.

Martin H, Claeys P, Gargaud M, Pinti DL & Selsis F (2006). Environmental Context. *Earth Moon Planets* **98,** 205–245.

Meakin PJ, Fowler MJ, Rathbone AJ, Allen LM, Ransom BR, Ray DE & Brown AM (2007). Fructose metabolism in the adult mouse optic nerve, a central white matter tract. *J Cereb Blood Flow Metab* **27,** 86–99.

Merchan-Perez A & Liberman MC (1996). Ultrastructural Differences Among Afferent Synapses on Cochlear Hair Cells: Correlations With Spontaneous Discharge Rate. *J Comp Neurol* **371,** 208–221.

Mikelberg FS, Drance SM, Schulzer M, Yidegiligne HM & Weis MM (1989). The Normal Human Optic Nerve: Axon Count and Axon Diameter Distribution. *Ophthalmology* **96,** 1325–1328.

Mulkidjanian AY, Bychkov AY, Dibrova D v., Galperin MY & Koonin E v. (2012). Origin of first cells at terrestrial, anoxic geothermal fields. *Proc Natl Acad Sci* **109**, e821-830

Mulkidjanian AY, Galperin MY, Makarova KS, Wolf YI & Koonin E v (2008). Evolutionary primacy of sodium bioenergetics. *Biol Direct*; DOI: 10.1186/1745-6150-3-13.

Mulkidjanian AY, Makarova KS, Galperin MY & Koonin E v. (2007). Inventing the dynamo machine: the evolution of the F-type and V-type ATPases. *Nature Reviews Microbiology 2007* **5,** 892–899.

Neumcke B & Stämpfli R (1982). Sodium currents and sodium-current fluctuations in rat myelinated nerve fibres. *J Physiol* **329,** 163–184.

Orkand RK (1986). Glial-interstitial fluid exchange. *Ann N Y Acad Sci* **481,** 269–272.

Pavelka M & Roth J (2010). Peripheral Nerve: Connective Tissue Components. *Functional Ultrastructure,* **2***,* 324–325.

Perge JA, Koch K, Miller R, Sterling P & Balasubramanian V (2009). How the Optic Nerve Allocates Space, Energy Capacity, and Information. *Journal of Neuroscience* **29,** 7917–7928.

Perge JA, Niven JE, Mugnaini E, Balasubramanian V & Sterling P (2012). Why Do Axons Differ in Caliber? *Journal of Neuroscience* **32,** 626–638.

Pinti DL (2005). The Origin and Evolution of the Oceans. In *Lectures in Astrobiology*, ed. Gargaud M, pp. 83–112. Springer, Berlin, Heidelberg.

Ransom CB, Ransom BR & Sontheimer H (2000). Activity-dependent extracellular K+ accumulation in rat optic nerve: the role of glial and axonal Na+ pumps. *J Physiol* **522,** 427.

Rich LR, Patrick JA, Hamner MA, Ransom BR & Brown AM (2020). A method for reducing animal use whilst maintaining statistical power in electrophysiological recordings from rodent nerves. *Heliyon* **6,** e04143.

Rokni D & Hochner B (2002). Ionic currents underlying fast action potentials in the obliquely striated muscle cells of the octopus arm. *J Neurophysiol* **88,** 3386–3397.

Rolfe DFS & Brown GC (1997). Cellular energy utilization and molecular origin of standard metabolic rate in mammals. *Physiol Rev* **77,** 731–758.

de Ronde CEJ, Channer DM deR., Faure K, Bray CJ, Spooner ETC, de Ronde CEJ, Channer DM deR., Faure K, Bray CJ & Spooner ETC (1997). Fluid chemistry of Archean seafloor hydrothermal vents: Implications for the composition of circa 3.2 Ga seawater. *GeCoA* **61,** 4025–4042.

Sanchez RM, Dunkelberger GR & Quigley HA (1986). The number and diameter distribution of axons in the monkey optic nerve. *Invest Ophthalmol Vis Sci* **27,** 1342–1350.

Schwarz JR (2021). Function of K2P channels in the mammalian node of Ranvier. *J Physiol* **599,** 4427–4439.

Schwarz JR, Glassmeier G, Cooper EC, Kao TC, Nodera H, Tabuena D, Kaji R & Bostock H (2006). KCNQ channels mediate IKs, a slow K+ current regulating excitability in the rat node of Ranvier. *J Physiol* **573,** 17-34.

Sherman SM, Norton TT & Casagrande VA (1975). X- and Y-cells in the dorsal lateral geniculate nucleus of the tree shrew (Tupaia glis). *Brain Res* **93,** 152–157.

Skulachev VP (1988). *Membrane Bioenergetics*. Springer-Verlag, Berlin.

Somjen GG (1979). Extracellular potassium in the mammalian central nervous system. *Annu Rev Physiol* **41,** 159–177.

Stassart RM, Möbius W, Nave KA & Edgar JM (2018). The Axon-Myelin Unit in Development and Degenerative Disease. *Front Neurosci*, **12**, 467.

Stiefel KM, Torben-Nielsen B & Coggan JS (2013). Proposed evolutionary changes in the role of myelin. *Front Neurosci*, 202.

Tanner AR, Fuchs D, Winkelmann IE, Gilbert MTP, Pankey MS, Ribeiro ÂM, Kocot KM, Halanych KM, Oakley TH, da Fonseca RR, Pisani D & Vinther J (2017). Molecular clocks indicate turnover and diversification of modern coleoid cephalopods during the Mesozoic Marine Revolution. *Proceedings of the Royal Society B: Biological Sciences*, **284,** e 20162818.

Vermeij GJ (1987). *Evolution and Escalation: An Ecological History of Life - Geerat J. Vermeij - Google Books*. Princeton University Press , Princeton, NJ.

Waxman SG (1980). Determinants of conduction velocity in myelinated nerve fibers. *Muscle Nerve* **3,** 141–150.

Williams RW & Chalupa LM (1983). An analysis of axon caliber within the optic nerve of the cat: evidence of size groupings and regional organization. *Journal of Neuroscience* **3,** 1554–1564.

Zang Y & Marder E (2021). Interactions among diameter, myelination, and the Na/K pump affect axonal resilience to high-frequency spiking. *Proc Natl Acad Sci.,* **118**, e2105795118

6 Publications and Presentations

6.1 Papers

Hopper, A.J., Beswick-Jones, H. & Brown, A.M. A color-coded graphical guide to the Hodgkin and Huxley papers. *Advances in Physiology Education,* 46 (2022) p.580-592

Hopper, A., Beswick-Jones, H. & Brown, A.M.. The Nernst equation: using physico-chemical laws to steer novel experimental design. *Advances in Physiology Education,* 46 (2022) p. 206-210

6.2 Conference appearances

NC3Rs 8th July 2022 Nottingham
A method for increasing experimental efficiency whilst maintaining statistical power: application to electrophysiological recordings from rodent optic nerve

Amy Hopper, Hana Beswick-Jones & Angus M Brown

Physiology Society 12-13th April 2022 Nottingham
Axon sub-population sensitivity to high frequency stimulus in adult mouse optic nerve

Amy Hopper, Hana Beswick-Jones & Angus M Brown